Global analysis of methionine oxidation provides a census of folding stabilities for the human proteome

Ethan J. Walker[1,2], John Q. Bettinger[1], Kevin A. Welle[3], Jennifer R. Hryhorenko[3], Sina Ghaemmaghami[1,3*]

[1]Department of Biology, University of Rochester, NY, 14627, USA

[2]Department of Biochemistry, University of Rochester Medical Center, NY, 14627, USA

[3]University of Rochester Mass Spectrometry Resource Laboratory, NY, 14627, USA

[*]Correspondence: sina.ghaemmaghami@rochester.edu (S.G.)

SUMMARY

The stability of proteins influences their tendency to aggregate, undergo degradation or become modified in cells. Despite their significance to understanding protein folding and function, quantitative analyses of thermodynamic stabilities have been mostly limited to soluble proteins in purified systems. We have used a highly multiplexed proteomics approach, based on analyses of methionine oxidation rates, to quantify stabilities of ~10,000 unique regions within ~3,000 proteins in human cell extracts. The data identify lysosomal and extracellular proteins as the most stable ontological subsets of the proteome. We show that the stability of proteins impacts their tendency to become oxidized and is globally altered by the osmolyte trimethylamine-N-oxide (TMAO). We also show that most proteins designated as intrinsically disordered retain their unfolded structure in the complex environment of the cell. Together, the data provide a census of the stability of the human proteome and validate a methodology for global quantitation of folding thermodynamics.

KEYWORDS

protein stability, protein folding, quantitative proteomics, methionine oxidation, intrinsically disordered proteins, osmolytes

INTRODUCTION

Within a cell, most proteins exist in a dynamic equilibrium between folded and unfolded conformations[1,2]. The free energy difference between these two states ($\Delta G_{folding}$ or 'thermodynamic folding stability') establishes the fraction of its population that is in a folded conformation at equilibrium[3]. Folding stabilities can impact the tendency of proteins to aggregate, oxidize or undergo degradation, and alterations in protein stabilities play a role in diverse biological processes and physiological disorders (e.g. aging and neurodegenerative proteinopathies)[4-8]. Despite their fundamental importance to protein function, the magnitude and span of folding stabilities within the proteome remain unclear. For example, estimations of the fraction of the proteome that harbors 'intrinsically disordered' domains are largely based on theoretical predictions and, with a few exceptions[9], have yet to be verified by proteome-wide experimental data[10].

Historically, quantitative measurements of protein folding stabilities have been conducted for proteins in purified systems using *in vitro* denaturation experiments that employ global folding probes such as circular dichroism or isothermal calorimetry[11]. Although these studies have made significant contributions to our understanding of folding thermodynamics, they have inherent limitations that mitigate their *in vivo* relevance. First, these studies have been biased towards well-folded stable protein model systems that can be easily expressed and purified. Hence, the thermodynamic folding parameters measured for well-studied folding models may not be representative of the proteome as a whole. Second, experiments conducted in purified systems typically do not account for the effects of interacting partners and other cellular factors

that may influence protein stabilities *in vivo*. Third, these methodologies are inherently low throughput and cannot be easily used to investigate protein stabilities on proteome-wide scales.

To address these shortcomings, a number of recently developed techniques have investigated protein folding patterns using probes that can be analyzed by mass spectrometry-based proteomics. Hydrogen/deuterium exchange (HX)[12,13], hydroxyl radical footprinting[14] and limited proteolysis[9,15-18] have been coupled with liquid chromatography-tandem mass spectrometry (LC-MS/MS) to provide proteome-wide measures of protein structure. These global studies have successfully investigated thermostabilities (melting temperatures), ligand binding interactions and conformational changes induced by environmental alterations. However, due in part to technical limitations inherent in each of these approaches, it has proven difficult to obtain measurements of thermodynamic folding stabilities ($\Delta G_{folding}$) on proteome-wide scales.

In this study, we globally measured protein folding stabilities by using methionine oxidation as a probe. This approach, referred to as Stability of Proteins from Rates of Oxidation (SPROX) and initially described by West and colleagues[19], offers a number of advantages that are particularly conducive to proteomic workflows. Methionine oxidation is a small, non-labile modification that can be readily coupled with chemical denaturation and is retained during the course of LC-MS/MS analyses. Selective oxidation of methionines allows for straightforward database searches, identification of modification sites and interpretation of oxidation kinetics. Furthermore, the use of chemical denaturants prevents the irreversible aggregation of proteins during the course of denaturation - a phenomenon that typically confounds thermal unfolding experiments.

To date, SPROX has been used to analyze the stability of individual intact proteins and to examine proteome-wide alterations in denaturation patterns induced by ligand binding[19-21]. Here, we have coupled SPROX with highly multiplexed tandem mass tagging (TMT) to obtain high-resolution denaturation curves - an approach we have termed high resolution SPROX (HR-SPROX). By analyzing HR-SPROX data in the context of thermodynamic protein folding models, we were able to measure localized $\Delta G_{folding}$ values on a proteome-wide scale.

RESULTS

HR-SPROX workflow

Figure 1 outlines the premise and workflow of HR-SPROX analyses and detailed methods are provided in Supplementary Information. Methionine is a readily oxidizable amino acid and can be converted to methionine sulfoxide by the oxidizing agent hydrogen peroxide (H_2O_2)[22]. The oxidation rate of a methionine residue within a protein is contingent on its local structural environment. Exposed methionines in unfolded regions oxidize faster than protected methionines in folded regions[23-25]. Thus, the energy difference between the folded and unfolded conformations ($\Delta G_{folding}$) can modulate the folding equilibrium and rate of methionine oxidation. The progressive addition of a chemical denaturant results in the unfolding of the protein (as $\Delta G_{folding}$ increases) and escalates the rate of oxidation. Monitoring the extent of oxidation (at a constant oxidation time) in the presence of increasing concentrations of a chemical denaturant produces a denaturation curve[19].

The SPROX denaturation curve can potentially provide four types of information: baseline oxidation, $[denaturant]_{1/2}$, $\Delta G_{folding}$ and m-value (Figure 1A). The level of baseline oxidation (the extent of oxidation induced by H_2O_2 in the absence of denaturant) provides a measure of the susceptibility of the methionine to oxidation in the context of the native protein. As we show below, this parameter is largely influenced by the level of solvent exposure of the methionine sidechain. The midpoint of denaturation ($[denaturant]_{1/2}$) is a model-independent parameter that provides the denaturant concentration required to unfold half of the protein population. For proteins that conform to a two-state folding model, where only the fully folded and fully unfolded conformations are significantly populated at all denaturant concentrations, the resulting sigmoidal denaturation curve can be interpreted in terms of the energy difference between the two conformations using the following equation (see Supplementary Information for formal derivation and assumptions):

$$fraction\ oxidized = 1/(1 + e^{\frac{\Delta G_{folding} + m\,[denaturant]}{RT}}) \quad (1)$$

Where $\Delta G_{folding}$ is the folding stability in the absence of denaturant, and the m-value is the slope of the linear relationship between $\Delta G_{folding}$ and [denaturant] in accordance to the linear extrapolation model of two-state folding (LEM)[26]. It has been shown that the m-value is correlated with the size and accessible surface area of the folding unit[27]. Thus, for proteins or domains that unfold in a two-state fashion, least-squares fitting the SPROX curve with the above equation can provide $\Delta G_{folding}$ measurements for the folding unit that encompasses the methionine.

Accurate determination of $\Delta G_{folding}$ values from HR-SPROX curves using LEM is contingent on the availability of a significant number of data points in the transition regions of the sigmoidal curves[26]. To obtain sufficient resolution required for analysis of a large number of polypeptides with diverse stabilities, we obtained data points at numerous denaturation concentrations (see below for exact statistics) and multiplexed the samples using tandem mass tags (TMT) (Figure 1B). Each methionine can potentially produce two HR-SPROX curves based on the disappearance of methionine or appearance of methionine sulfoxide as a function of denaturant concentration. For a given methionine, these two curves are expected to be mirror images of one another, providing two independent datasets for analysis of its localized stability.

It should be noted that methionine residues have a tendency to become oxidized in the cell or during mass spectrometric analysis, even in the absence of H_2O_2. However, the level of such spurious oxidation is minimal relative to the forced oxidation induced by H_2O_2. Furthermore, this background oxidation is expected to be constant at all denaturant concentrations and does not influence the measurements of normalized fractional oxidation.

Analysis of purified lysozyme validates the accuracy of $\Delta G_{folding}$ measurements by HR-SPROX

We first validated the HR-SPROX approach by analyzing purified lysozyme, a well-studied two-state protein folding model. Lysozyme has three buried tryptophan residues whose fluorescence emission spectra change upon denaturation (Figure 2A). A protected methionine resides in the same region of the protein, enabling parallel

analysis of stability by HR-SPROX. We obtained fluorescence and HR-SPROX denaturation curves using guanidine hydrochloride (GdmCl) as a denaturant. The experiments were carried out at room temperature at pH 7.4. Figure 2B compares the denaturation curves obtained by fluorescence and HR-SPROX for a methionine-containing tryptic peptide that also encompasses two of the buried tryptophan residues. Analysis of the two denaturation curves with the two-state folding model provides similar measurements for $[GdmCl]_{1/2}$, m-value and $\Delta G_{folding}$. These values are also consistent with previous stability measurements obtained for lysozyme under similar conditions[28].

HR-SPROX enables proteome-wide analysis of folding thermodynamics in human fibroblast extracts

We next extended our analysis to the proteome-wide investigation of complex extracts. Human diploid fibroblasts expressing the catalytic component of human telomerase (HCA2-hTert)[29] were grown to a contact-inhibited quiescent state in culture and extracts were obtained under non-denaturing conditions. A series of HR-SPROX analyses were carried out with GdmCl concentrations ranging from 0 to 3 M (Figure 3A). The experiments included five technical replicates obtained from two biological replicates, with each technical replicate being exposed to 30 denaturant concentrations and tagged with three different sets of 10-plex TMTs prior to LC-MS/MS analysis. Together, the data provided quantitative information for 10,412 unique methionine-containing peptides (in unoxidized and/or oxidized forms) mapped to 3,158 protein groups (Table 1, Supplementary Tables 1-3). All raw and processed data have been deposited to the ProteomeXchange Consortium via the PRIDE[30] partner repository with the dataset identifier PXD011456 (Username: reviewer84819@ebi.ac.uk Password: dmGTnZAy).

The H_2O_2 concentrations and oxidation times used in our experiments were sufficient to oxidize exposed methionines to methionine sulfoxides (Met-O) but did not lead to the formation of significant levels of methionine sulfones (Met-O_2) (Figure S1). The only other oxidized residue that was detectable at appreciable levels was sulfonic acid (Cys-O_3). However, levels of sulfonic acid-containing peptides were significantly lower than methionine sulfoxide-containing peptides and their formation did not result in any calculation bias in measurements of methionine oxidation (Figure S1).

We initially analyzed methionine oxidation levels in individual experiments and showed that there was a significant correlation between replicate experiments (Figure S2). Additionally, there was a significant correlation between denaturation curves of individual peptides independently obtained from disappearance of methionines and appearance of methionine sulfoxides (Figure S2). Given that replicate experiments were in general agreement with each other, we combined all available data (all replicates, encompassing measurements of oxidized and/or unoxidized peptides based on availability) to obtain high resolution denaturation curves for individual peptides. After merging datasets, the number of denaturant concentration points analyzed for individual methionine-containing peptides ranged from 10 to 300, with a median of 50 (Figure S3).

As an example, Figure 3B illustrates a HR-SPROX denaturation curve for a protected methionine residue in ADP-ribosylhydrolase. We noticed that although individual TMT data points for a given peptide generally overlapped and had consistent trends, outliers were typically present and heavily biased subsequent least-squares regression analyses of the denaturation curves. We therefore obtained moving averages of the denaturation data and used the resulting smoothed plots to conduct least squares

regression analyses (Figure 3B). The baseline oxidation, $[GdmCl]_{1/2}$, m-value and $\Delta G_{folding}$ measurements for individual methionine-containing peptides are tabulated in Supplementary Table 4.

Baseline methionine oxidation levels correlate with secondary structure and solvent accessibilities

We first focused on analysis of baseline oxidation levels in the absence of denaturant. The data indicated that the distribution of baseline oxidation levels within the proteome is remarkably bimodal, with approximately half of the methionines forming a relatively well-protected population and half forming a poorly protected population (Figure 4A). Based on these measurements, we set out to identify sequence and structural parameters that correlate with methionines' susceptibility to oxidation.

We did not find strong correlations between methionine oxidation and identities of neighboring residues in the primary sequence, beyond slightly decreased oxidation levels near hydrophobic residues (Figure 4B, S4). As discussed below, we can rationalize this trend by considering that hydrophobic residues are more likely to be in the protein core where methionines would lack exposure to solvent and thus be less susceptible to oxidation. Alternatively, as has been noted previously, the direct interaction of the methionine sidechain with aromatic residues may decrease the reactivity of the sulfur atom with oxygen[31].

We next cross-referenced baseline oxidation levels to the secondary structure context of the methionine residues using the Define Secondary Structure of Proteins (DSSP) analysis of corresponding protein databank (PDB) structures[32]. Structural data mapped

to 1,016 proteins in our dataset indicated that highly oxidizable methionines tend to be contained in turns, bends and unstructured coils, whereas more protected methionines tended to be in rigid secondary structure elements such as β-strands and α-helices (Figure 4C, Supplementary Table 5). We subsequently used PDB structures to measure the solvent accessible surface area (SASA) of methionines using the VMD molecular visualization program[33]. We observed a very strong positive correlation between the SASA of a methionine residue and its susceptibility to oxidation (Figure 4D, Supplementary Table 5). Together, the data provide proteome-wide evidence that secondary structure context and solvent accessibilities of methionine residues are the primary determinants of their susceptibility to oxidation. This trend had been previously noted for a limited number of individual proteins[25].

Intrinsically disordered proteins are highly prone to oxidation in cell extracts

A large number of protein regions and domains have been classified as *intrinsically disordered*, primarily based on lack of evidence for structure in crystallography or NMR studies, or low complexity patterns of amino acid usage in their primary sequence[34]. However, it is unclear what fraction of these sites retain their disorder in the complex intracellular environment of the cell where they could potentially be interacting with binding partners and other stabilizing factors. Given the strong correlation between localized structure and methionine oxidation established above, we assessed the baseline oxidation levels of methionines within regions classified as *disordered* in a curated database of intrinsically disordered proteins (MobiDB)[35]. Our analysis indicated that methionines within regions classified as *disordered* are significantly more prone to oxidation than those classified as *structured* (Figure 4E, Supplementary Table 5). This

suggests that as a group, proteins that have been classified as *intrinsically disordered* mostly retain this property in crude extracts where they could potentially be interacting with stabilizing factors and binding partners. Thus, methionine oxidation rates can potentially help resolve ambiguities where conflicting evidence exists regarding the *structured/disordered* designation of a protein region.

Susceptibility to oxidation is enriched in specific gene ontologies

We conducted gene ontology (GO) enrichment analyses to identify GO categories that were statistically enriched in protected or exposed methionines (Figure 4F, S5, Supplementary Table 6). GO categories most enriched in protected methionines included mitochondrial proteins, proteins involved in oxidation-reduction reactions and ATP synthesis. It is notable that these categories contain proteins that are particularly exposed to reactive oxygen species (ROS) within the cell. It is possible that the prevalence of protected methionines in these proteins is an adaptive response to safeguard against ROS-induced oxidative damage. Among the GO categories most enriched in exposed methionines were cytoskeletal proteins. It has been shown that enzyme-mediated methionine oxidation is a regulatory mechanism for cytoskeletal dynamics. MICAL proteins are F-actin disassembling factors that modify the actin cytoskeleton by oxidizing two conserved methionine residues in actin[36,37]. Our data indicate that not only are MICAL-targeted methionines highly prone to oxidation (Figure 5A), but that as a group, cytoskeletal proteins contain an atypically large number of exposed methionines that could potentially be targetable by other oxygenases[38].

HR-SPROX uncovers proteome-wide distributions of $[GdmCl]_{1/2}$, $\Delta G_{folding}$ and m-values

We next focused on analyzing thermodynamic folding parameters based on peptide HR-SPROX denaturation curves. We limited our analyses to peptides that contained protected methionines (conservatively defined as having a baseline oxidation levels less 0.5) and were well fit by a two-state folding model (r^2>0.9). This subset consisted of 1,798 peptides mapped to 991 proteins (Figure 5A). The distribution of $\Delta G_{folding}$, m-values, $[GdmCl]_{1/2}$ values are plotted in Figure 5B. The median stability for the analyzed peptides was -4.7 kcal/mol. It is interesting to note that this value represents a somewhat lower stability in comparison to stabilities previously measured by low-throughput analyses for most purified folding model systems[39]. It is likely that previous folding models (e.g. lysozyme) have been somewhat biased towards highly stable and soluble proteins that tend to be more abundant and easier to express or purify from source. Our data indicate that the overall stability of the proteome is even more marginal than previously proposed[40] and much of the proteome can be unfolded by the removal of one or few favorable non-covalent interactions from the native structure.

Protein stability is elevated in specific gene ontologies

We conducted gene ontology (GO) analyses to identify protein categories that are statistically enriched in highly stable or highly unstable regions as determined by $[GdmCl]_{1/2}$ and $\Delta G_{folding}$ measurements of their methionine residues (Figure 5C-D, S6, Supplementary Table 6). Among the most stable subsets of the proteome were proteins localized to the lysosomal lumen and extracellular space. Unfolding of target proteins in the denaturing environment of the lysosome is known to be required for their hydrolysis[41]. It is therefore likely that resident proteins of the lysosome have evolved to

be resistant to denaturation. Similarly, proteins localized to the oxidizing environment of the extracellular space are enriched in stabilizing disulfide bonds.

Among the least stable subsets of the proteome were ATP binding proteins and ribosomal proteins. At ATP concentrations present in cell extracts, many ATP binding proteins may exist in ATP-unbound forms that are predicted to be less stable than the ATP-bound forms[42]. At higher ATP concentrations, the binding equilibrium may shift to the bound form, resulting in ligand-induced stabilization. Similarly, ribosomal proteins are stabilized by stoichiometric association to form the intact small and large subunits of the ribosome. During the course of chemical denaturation, as the higher order structure of the ribosome is disrupted, orphaned ribosomal proteins appear to be relatively thermodynamically unstable.

Protein stability impacts the rate of oxidation for a subset of the proteome

We next analyzed the relationship between folding stability and baseline methionine oxidation (Figure 5E). The data indicated that $\Delta G_{folding}$ is not a strong predictor of baseline susceptibility to oxidation for two-state proteins that are relatively stable ($\Delta G_{folding} < -1.5$ kcal/mol). However, once protein stability declines beyond a minimum threshold, baseline methionine oxidation rates begin to rise. Thus, in unstable protein regions, oxidation from the unfolded state is the dominant pathway for oxidation, and the rate of oxidation is contingent on the folding equilibrium. Conversely, in stable protein regions, where the folding equilibrium is heavily shifted towards the native state, oxidation occurs primarily from the folded structure. In this regime, the rate of oxidation

is independent of the folding equilibrium and instead appears to be limited by the solvent accessibility of the methionine in the native state.

HR-SPROX enables analysis of inter- and intra-domain variability in stability

An important feature of the HR-SPROX analysis is that it can potentially provide localized stability information within proteins. In theory, different methionines within the same protein provide independent and localized stability probes. In a multi-domain protein where each domain is an independent cooperative folding unit[43], different methionines within the same domain are expected to report similar stabilities. To assess this feature of our data, we examined intra-domain variability in our stability measurements. In general, we found that different methionines within the same domain have similar stabilities (Figure 6).

An example of this trend is shown for the cytoskeletal protein talin (Figure 6A). Talin is a large, amphipathic multi-domain protein that forms a mechanical linkage between integrins and the cellular cytoskeleton. The interaction between talin domains and vinculin in focal adhesions is force-dependent and is thought to occur through mechanical unfolding of specific talin domains that expose cryptic vinculin binding sites. To identify potential binding sites, mechanical stabilities of individual talin domains have been previously investigated by single molecule atomic force microscopy (smAFM)[44-46]**.** Here, we were able to track the stability and solvent exposure of 16 of the 18 domains in talin. Our data are largely consistent with the smAFM findings. We found that domains shown to have low mechanical stability by smAFM, including the linker region, R3 and R4 are solely composed of highly exposed methionines. Conversely, domains that have been shown to be highly stable, such as R5 and R9 contained protected and

stable methionines. Additionally, our analysis provided thermodynamic data on domains that have not been previously studied by smAFM. For example, we identified R13 as another highly stable talin domain. These results highlight the ability of HR-SPROX to analyze localized thermodynamic stability data for large multi-domain proteins that are difficult to study by traditional protein denaturation experiments.

Within individual talin domains where multiple methionine-containing peptides could be identified, the stability trends were in good agreement with each other (see overlap between protected methionine curves in Figure 6A). To examine the generality of this trend, we used the Pfam database of protein domains[47] to globally define domain boundaries within our dataset and analyzed intra-domain variability in our measurements. The analysis indicated that variabilities in $[GdmCl]_{1/2}$, $\Delta G_{folding}$ and m-values were significantly lower within domains in comparison to variabilities of the parameters within the overall proteome (Figure 6B-E). The results are consistent with the idea that most domains behave as independent cooperative folding units.

The chemical chaperone TMAO has variable stabilizing effects on the proteome

To determine whether HR-SPOX is capable of monitoring changes in protein stability induced by environmental alterations, we repeated our analyses in the presence of the chemical chaperone trimethylamine-N-oxide (TMAO). TMAO is an amine-oxide osmolyte[48]. It is found in the tissues of a variety of marine organisms where it is thought to counteract the destabilizing effects of urea and pressure on proteins. It has been postulated that TMAO stabilizes proteins by increasing the free energy of the unfolded state through solvent exclusion effects, thus shifting the folding equilibrium towards the native state[49,50]. Although the stabilizing effects of TMAO had previously been observed

for a number of proteins[51,52], the selectivity of its stabilizing effects have not been investigated on a proteome-wide scale. We conducted a limited HR-SPROX analysis in the presence of 1 M TMAO (Figure S7) and compared the baseline oxidation levels, $[GdmCl]_{1/2}$, $\Delta G_{folding}$ and m-values of methionine-containing peptides to untreated controls (Figure 7, S7). Overall, we observed that TMAO decreased baseline oxidation levels and increased the stability of the proteome, although the magnitudes of these effects were variable between proteins (Figure7A).

Our data indicated that TMAO decreased baseline oxidation levels of protected methionines within unstable proteins ($\Delta G_{folding}$>-1.5 kcal/mol), but that this effect was diminished for more stable proteins (Figure 7B-C). This trend is consistent with the idea that unlike stable protein regions, methionine oxidation in unstable protein regions occurs primarily from the unfolded state. Hence, modulation of the folding equilibrium by a chemical chaperone can effectively decrease oxidation rates in unstable protein regions (see above and Figure 5E). However, TMAO did not significantly decrease the oxidation rates of most highly exposed methionines, indicating that most unstructured regions within proteins (including regions with non-rigid secondary structures, high solvent accessibility and those characterized as *intrinsically disordered*) do not transform to stably folded structures in the presence of 1 M TMAO (Figure 7C, S7). Although our experiments did not investigate the efficacy of TMAO at higher concentrations, the results indicate that at levels where it has a significant impact on the stability of structured proteins (Figure 7D-F), TMAO is not able to impose structure on the majority of disordered regions within the proteome.

DISCUSSION

In this study, we investigated the thermodynamic folding stability of the human proteome using methionine oxidation as a probe. Our data indicate that rates of methionine oxidation are correlated to localized structure and amenable to detection and quantitation by bottom-up proteomics. However, this approach has at least two important limitations. First, the analysis is limited to tryptic peptides that contain methionines, which is one of the least abundant residues in natural proteins. For example, in our analyses, although we were able to detect a total of 60,776 unique peptides in our combined experiments, only 19% contained methionines and could be analyzed by HR-SPROX. Second, methionine oxidation is not a benign modification and may in itself impact folding stability. Thus, oxidation of one methionine could artifactually alter the localized stability of a second methionine located elsewhere in the same protein. Although we cannot rule out this possibility for any one protein or domain, our proteome-wide data indicate that a significant fraction of domains unfold cooperatively in a two-state fashion, and within these domains, different methionines generally report similar stabilities. It is also important to note that methionine oxidation represents a significantly less disruptive modification in comparison to alternative proteomic approaches for analysis of protein structure based on limited proteolysis or indiscriminate radical footprinting.

Using HR-SPROX we were able to quantify the susceptibility of a large number of methionines to oxidation by H_2O_2. Our results indicate that the distribution of methionine oxidation susceptibilities is strikingly bimodal. Methionines within the human proteome

appear to be divided into two roughly equal-sized groups: solvent exposed methionines that are highly prone to oxidation, and buried methionines that are protected from oxidation. Methionines are hydrophobic residues that would be expected to reside primarily in the cores of proteins based solely on their chemical properties. However, it has been suggested that exposed surface methionines can play a protective role by acting as sinks for reactive oxygen species (ROS)[53]. Within the cell, the oxidation of methionines is enzymatically reversible and their reduction by methionine sulfoxide reductases (MSRs), and subsequent formation of NADPH, forms a complete redox cycle[54,55]. Thus, reversible oxidation of surface methionines can act as a removal mechanism for cellular ROS and prevent the irreversible oxidation of other biomolecules[53]. In support of this idea, our data provides global experimental evidence for the high prevalence of exposed oxidation-prone methionines in the human proteome.

Our analysis was able to measure thermodynamic folding stabilities ($\Delta G_{folding}$) for ~1,800 protein regions that contain highly protected methionines and unfold in accordance with a two-state model. To the best of our knowledge, this analysis represents the largest survey of thermodynamic protein stabilities conducted to date. The median stability measured in our analysis is ~4.7 kcal/mol, which is lower than the majority of the folding models studied to date in purified systems. Whether this observation reflects an experimental bias towards more stable folding models in previous studies, or presence of cellular factors in cell extracts that alter protein stabilities in comparison to purified conditions remains to be determined. Nonetheless, the data highlight the remarkable range of stabilities within the proteome and suggest that stability is a physical property

that has adapted to meet the specific functional needs of proteins. For example, our data highlight lysosomal and extracellular proteins as two subsets of the proteome that have evolved high stabilities, likely due to the physical demands of their local environments.

Our proteome-wide data also uncovered an important relationship between folding stability and methionine oxidation. We showed that in general there are two oxidation pathways for buried methionine residues. Oxidation can occur rapidly from the denatured state or more slowly from the folded state. Most buried and protected methionines reside in structured regions with stabilities that are high enough to heavily favor oxidation through the native state. However, ~10% of protected methionines analyzed in our study were located in regions that were sufficiently unstable ($\Delta G_{folding}$>-1.5 kcal/mol) to favor oxidation through the denatured state. The oxidation rate of this subset of the proteome is contingent on folding stability and can be diminished by stabilizing factors such as chemical chaperones (e.g. TMAO).

It has long been known that TMAO stabilizes proteins in saltwater fish, sharks, crustaceans and molluscs[56]. It is thought that this activity may counteract the destabilizing effects of urea and pressure in deep-sea animals. However, the exact physical mechanism of the stabilizing effects of TMAO remains under active investigation. It has been shown that interactions between TMAO and the peptide backbone raises the energy of unfolded structures and energetically favors the folded state[49,57]. Here, we have shown that TMAO does indeed stabilize much of the proteome. However, the magnitude of its effect is variable between proteins and domains. Our experiments have quantified the effects of TMAO on diverse protein

substrates and the results may provide a useful resource for evaluating putative mechanisms of stabilization by this osmolyte. More generally, this study demonstrates that HR-SPROX can be used to identify client-sets of chaperones by globally quantifying their effects on protein folding stabilities.

It has been predicted that ~30% of the human proteome contains regions that can be classified as intrinsically disordered (IDPs)[10]**.** However, investigating the prevalence and properties of these regions within the cellular environment has proven challenging. In theory, the presence of interacting partners and molecular chaperones in cell extracts may impose structure on regions that otherwise appear disordered in purified systems. Here, we used HR-SPROX to probe the structure and stability of regions classified as IDPs in crude extracts. Our data indicate that in comparison to the rest of the proteome, methionines in IDPs are highly prone to oxidation. These results suggest that most proteins designated as IDPs remain relatively unstructured even in crude extracts.

Our data also indicate that the addition of TMAO does not alter the oxidation properties of most IDPs, suggesting that most disordered regions can not be significantly folded by the addition of 1M concentrations of this osmolyte. As described above, TMAO is thought to modulate the equilibrium constant between the unfolded and the native state of stably folded proteins. However, this mechanism of action is contingent on the existence of localized energy minima representative of denatured and native states. Our data suggest that the folding energy landscapes of most IDPs may not contain localized minima representative of unique native states. Thus, IDPs may represent fundamentally different structures in comparison to “unstable proteins”. While the folding equilibrium of the latter can be altered in favor of a native state by the addition of osmolytes such as

TMAO, the former inherently lack a native structure and are incapable of achieving a singular folded state even in the presence of stabilizing agents.

Together, our data validate a global methodology for quantitative analysis of protein stability and provide a proteome-wide census of $\Delta G_{folding}$ for the human proteome. This approach may prove useful in investigating proteome-wide trends in folding stabilities and can be employed in future studies to investigate the stabilizing effects of molecular chaperones, characterize the impact of environmental stresses on protein folding, and examine cross-species conservation of folding thermodynamics.

SUPPLEMENTAL INFORMATION

Supplemental information include detailed experimental methods, seven figures and seven data tables.

ACKNOWLEDGEMENTS

We thank Dr. Michael Fitzgerald, Dr. Mark Dumont and members of the Ghaemmaghami and Fu labs for helpful comments on the manuscript. This work was supported by grants from the National Science Foundation (MCB-1350165 CAREER) and National Institutes of Health (R35 GM119502-01, T32 GM068411, 1S100D021486-01, 1S10OD025242-01).

AUTHOR CONTRIBUTIONS

E.W. and S.G. conceptualized the study, E.W., K.W., S.G. designed the experiments, E.W., K.W., J.H. performed the experiments, E.W., J.B., K.W., S.G. designed and carried out the data analysis, E.W. and S.G. wrote the manuscript.

DECLARATION OF INTERESTS

The authors declare no competing interests.

FIGURES

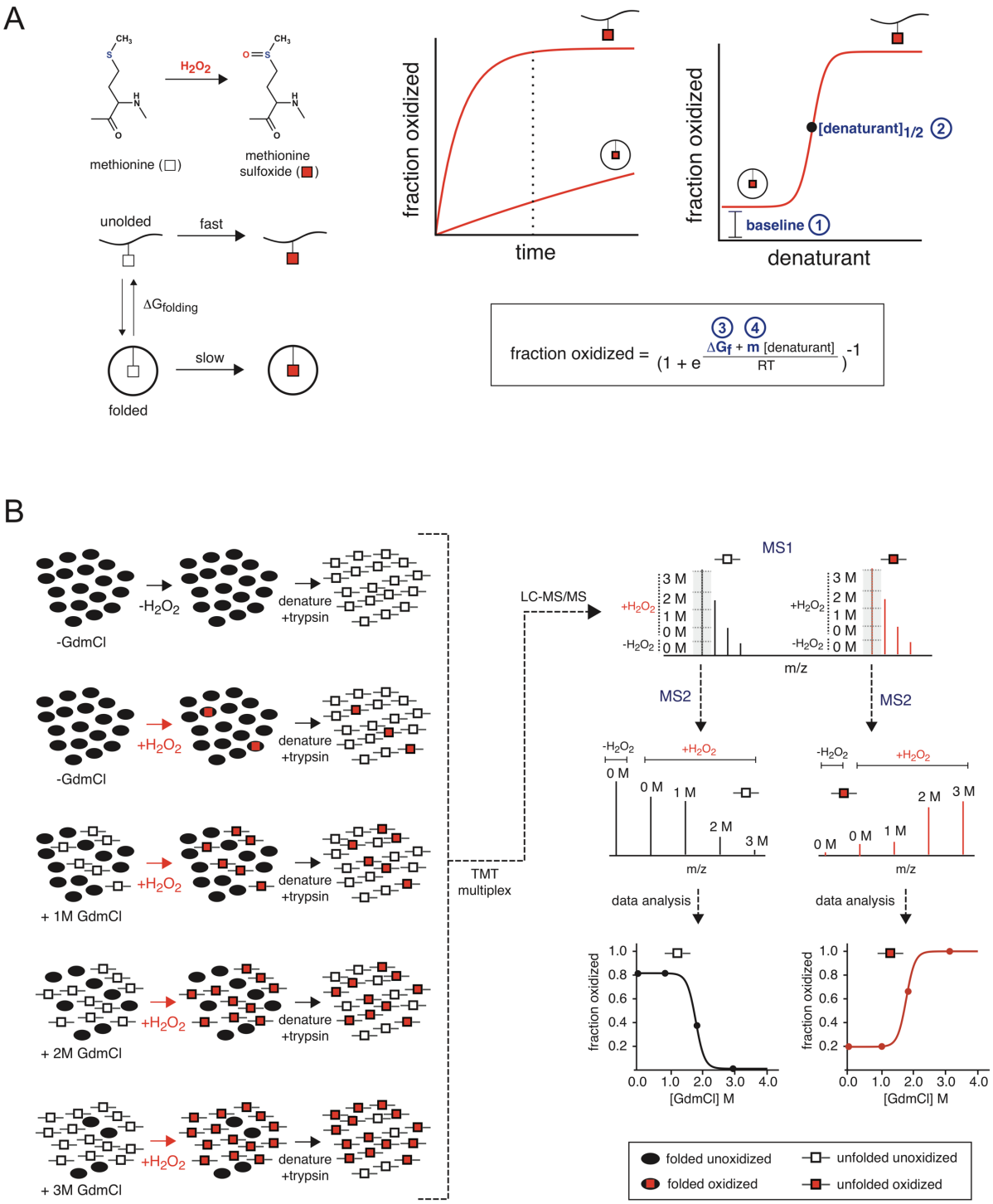

Figure 1

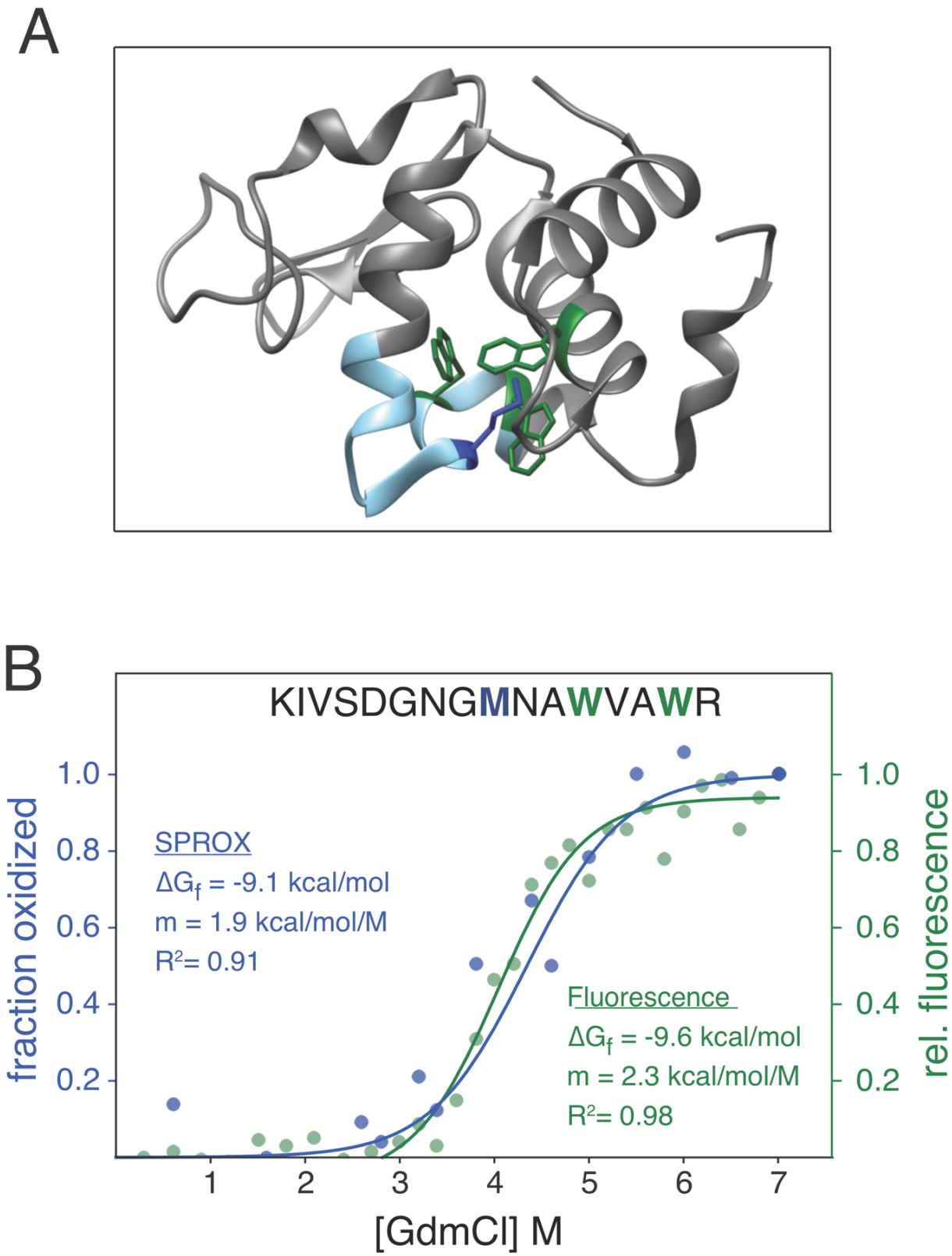
A
B
KIVSDGNGMNAWVAWR
SPROX
ΔGf = -9.1 kcal/mol
m = 1.9 kcal/mol/M
R2= 0.91
Fluorescence
ΔGf = -9.6 kcal/mol
m = 2.3 kcal/mol/M
R2= 0.98
fraction oxidized
rel. fluorescence
[GdmCl] M
1.0
0.8
0.6
0.4
0.2
1
2
3
4
5
6
7

Figure 2

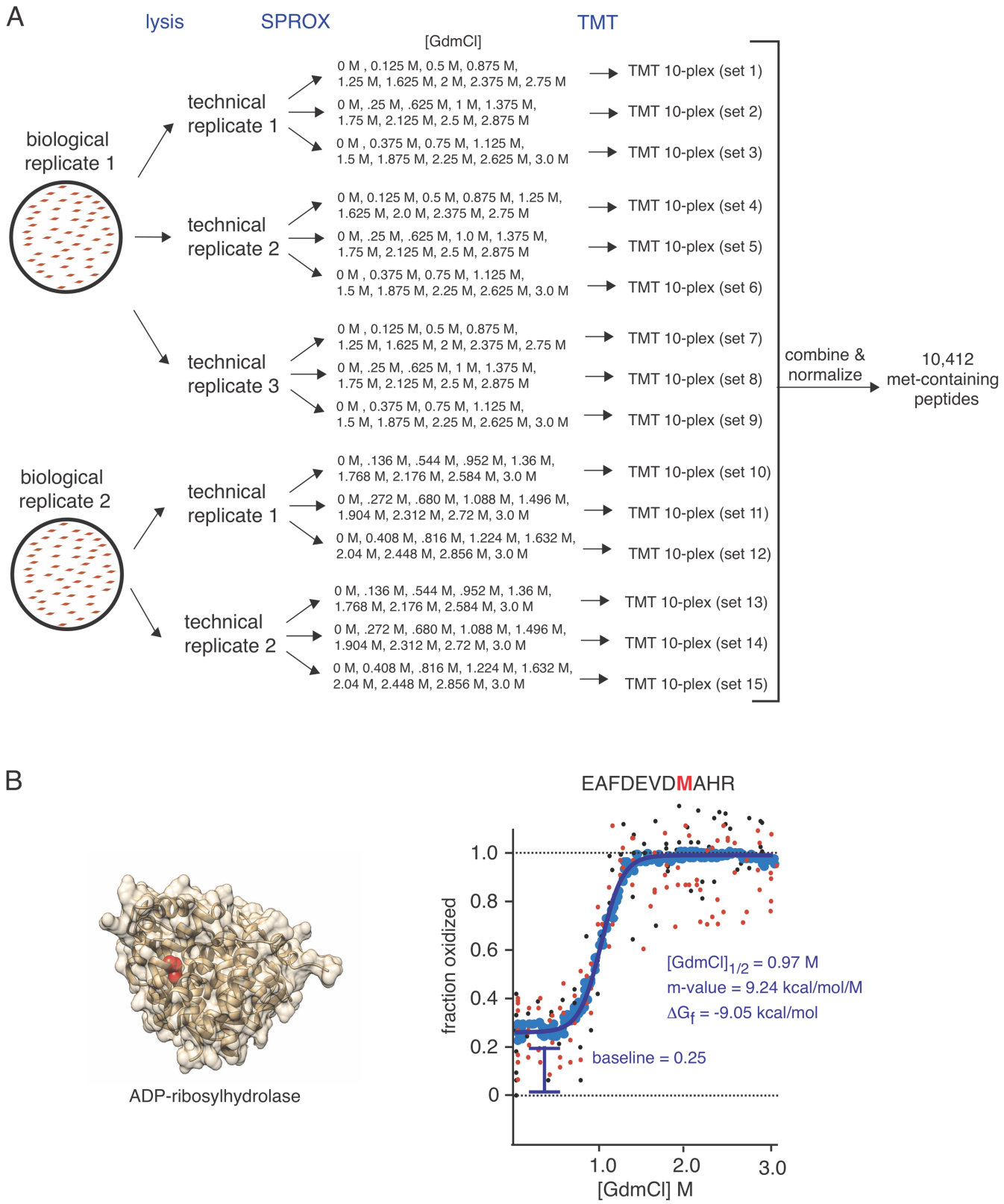
A
lysis
SPROX
TMT
[GdmCl]
biological replicate 1
technical replicate 1
technical replicate 2
technical replicate 3
biological replicate 2
technical replicate 1
technical replicate 2
0 M , 0.125 M, 0.5 M, 0.875 M, 1.25 M, 1.625 M, 2 M, 2.375 M, 2.75 M
0 M, .25 M, .625 M, 1 M, 1.375 M, 1.75 M, 2.125 M, 2.5 M, 2.875 M
0 M , 0.375 M, 0.75 M, 1.125 M, 1.5 M, 1.875 M, 2.25 M, 2.625 M, 3.0 M
0 M, 0.125 M, 0.5 M, 0.875 M, 1.25 M, 1.625 M, 2.0 M, 2.375 M, 2.75 M
0 M, .25 M, .625 M, 1.0 M, 1.375 M, 1.75 M, 2.125 M, 2.5 M, 2.875 M
0 M , 0.375 M, 0.75 M, 1.125 M, 1.5 M, 1.875 M, 2.25 M, 2.625 M, 3.0 M
0 M , 0.125 M, 0.5 M, 0.875 M, 1.25 M, 1.625 M, 2 M, 2.375 M, 2.75 M
0 M, .25 M, .625 M, 1 M, 1.375 M, 1.75 M, 2.125 M, 2.5 M, 2.875 M
0 M , 0.375 M, 0.75 M, 1.125 M, 1.5 M, 1.875 M, 2.25 M, 2.625 M, 3.0 M
0 M, .136 M, .544 M, .952 M, 1.36 M, 1.768 M, 2.176 M, 2.584 M, 3.0 M
0 M, .272 M, .680 M, 1.088 M, 1.496 M, 1.904 M, 2.312 M, 2.72 M, 3.0 M
0 M, 0.408 M, .816 M, 1.224 M, 1.632 M, 2.04 M, 2.448 M, 2.856 M, 3.0 M
0 M, .136 M, .544 M, .952 M, 1.36 M, 1.768 M, 2.176 M, 2.584 M, 3.0 M
0 M, .272 M, .680 M, 1.088 M, 1.496 M, 1.904 M, 2.312 M, 2.72 M, 3.0 M
0 M, 0.408 M, .816 M, 1.224 M, 1.632 M, 2.04 M, 2.448 M, 2.856 M, 3.0 M
TMT 10-plex (set 1)
TMT 10-plex (set 2)
TMT 10-plex (set 3)
TMT 10-plex (set 4)
TMT 10-plex (set 5)
TMT 10-plex (set 6)
TMT 10-plex (set 7)
TMT 10-plex (set 8)
TMT 10-plex (set 9)
TMT 10-plex (set 10)
TMT 10-plex (set 11)
TMT 10-plex (set 12)
TMT 10-plex (set 13)
TMT 10-plex (set 14)
TMT 10-plex (set 15)
combine & normalize
10,412 met-containing peptides
B
ADP-ribosylhydrolase
EAFDEVDMAHR
fraction oxidized
1.0
0.8
0.6
0.4
0.2
0
[GdmCl]1/2 = 0.97 M
m-value = 9.24 kcal/mol/M
ΔGf = -9.05 kcal/mol
baseline = 0.25
1.0
2.0
3.0
[GdmCl] M

Figure 3

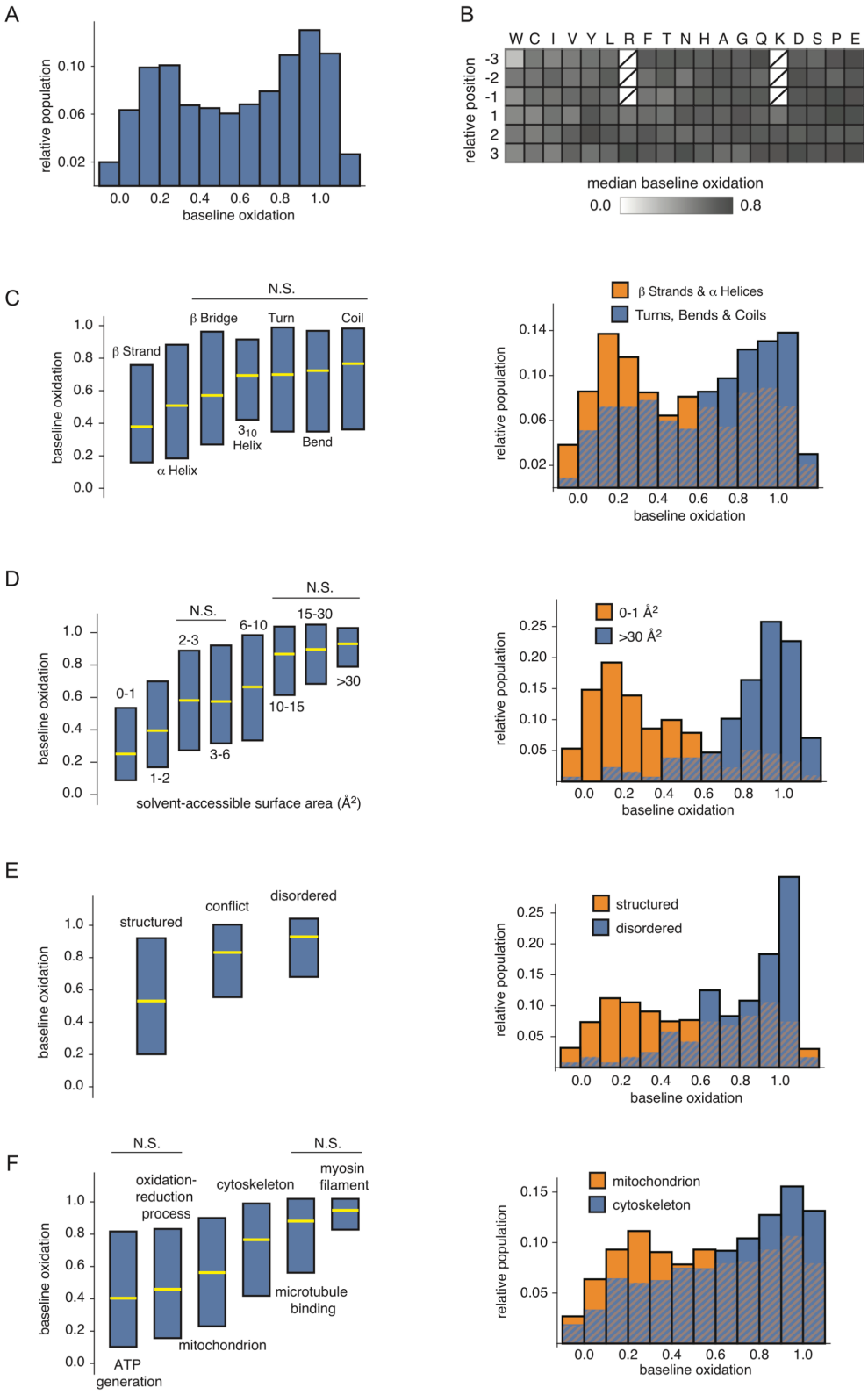
A
relative population
0.10
0.06
0.02
0.0 0.2 0.4 0.6 0.8 1.0
baseline oxidation
B
W C I V Y L R F T N H A G Q K D S P E
relative position
-3
-2
-1
1
2
3
median baseline oxidation
0.0
0.8
C
N.S.
β Strand
β Bridge
Turn
Coil
α Helix
3₁₀ Helix
Bend
baseline oxidation
β Strands & α Helices
Turns, Bends & Coils
relative population
baseline oxidation
D
N.S.
N.S.
0-1
1-2
2-3
3-6
6-10
10-15
15-30
>30
solvent-accessible surface area (Å²)
baseline oxidation
0-1 Å²
>30 Å²
relative population
baseline oxidation
E
structured
conflict
disordered
baseline oxidation
structured
disordered
relative population
baseline oxidation
F
N.S.
N.S.
ATP generation
oxidation-reduction process
mitochondrion
cytoskeleton
microtubule binding
myosin filament
baseline oxidation
mitochondrion
cytoskeleton
relative population
baseline oxidation

Figure 4

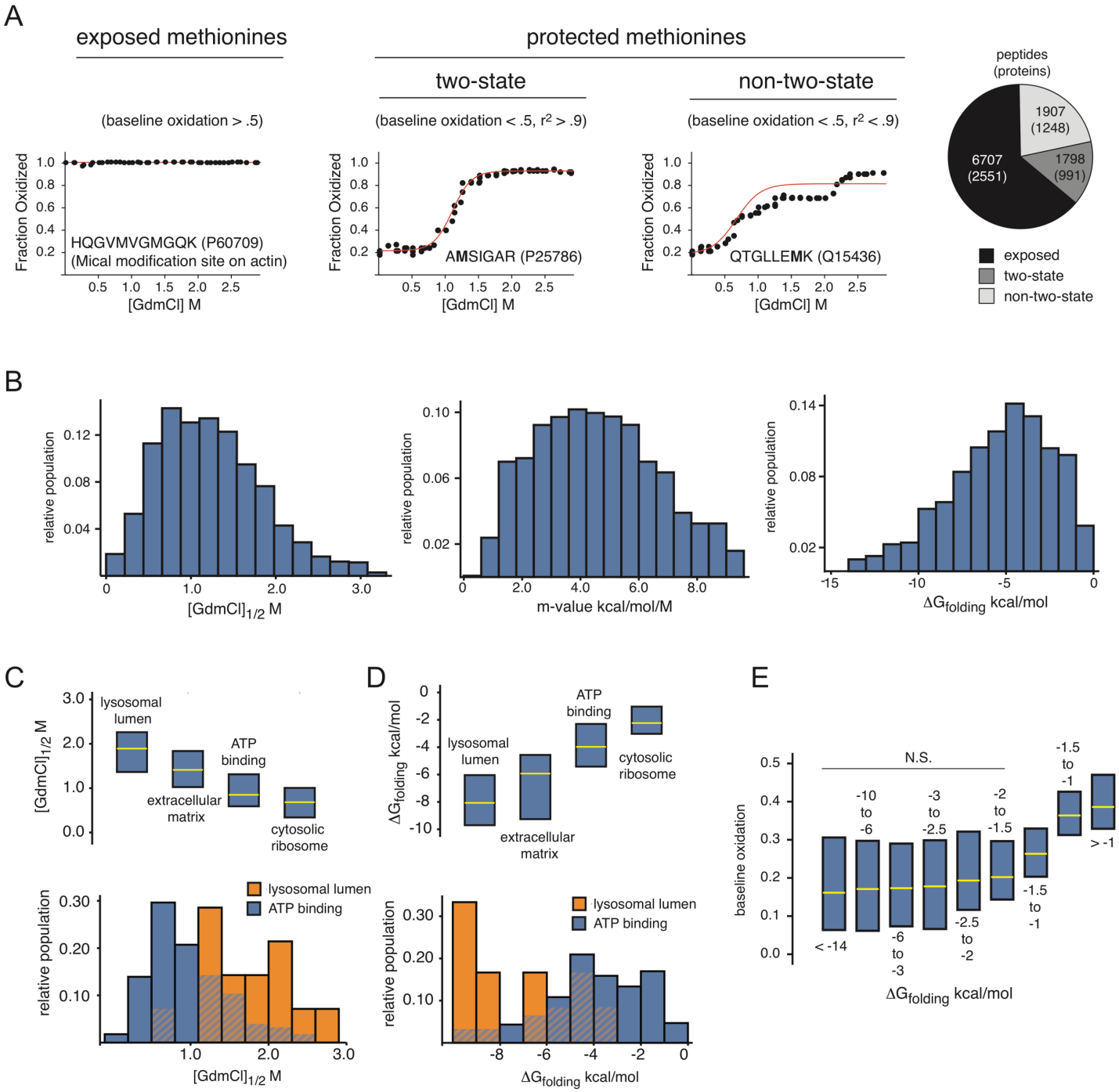
A
exposed methionines
protected methionines
two-state
non-two-state
(baseline oxidation > .5)
(baseline oxidation < .5, r2 > .9)
(baseline oxidation < .5, r2 < .9)
Fraction Oxidized
HQGVMVGMGQK (P60709)
(Mical modification site on actin)
AMSIGAR (P25786)
QTGLLEMK (Q15436)
[GdmCl] M
peptides
(proteins)
1907
(1248)
6707
(2551)
1798
(991)
exposed
two-state
non-two-state
B
relative population
[GdmCl]1/2 M
m-value kcal/mol/M
ΔGfolding kcal/mol
C
[GdmCl]1/2 M
lysosomal
lumen
ATP
binding
extracellular
matrix
cytosolic
ribosome
lysosomal lumen
ATP binding
D
ΔGfolding kcal/mol
E
N.S.
baseline oxidation
< -14
-10
to
-6
-6
to
-3
-3
to
-2.5
-2.5
to
-2
-2
to
-1.5
-1.5
to
-1
-1.5
to
-1
> -1

Figure 5

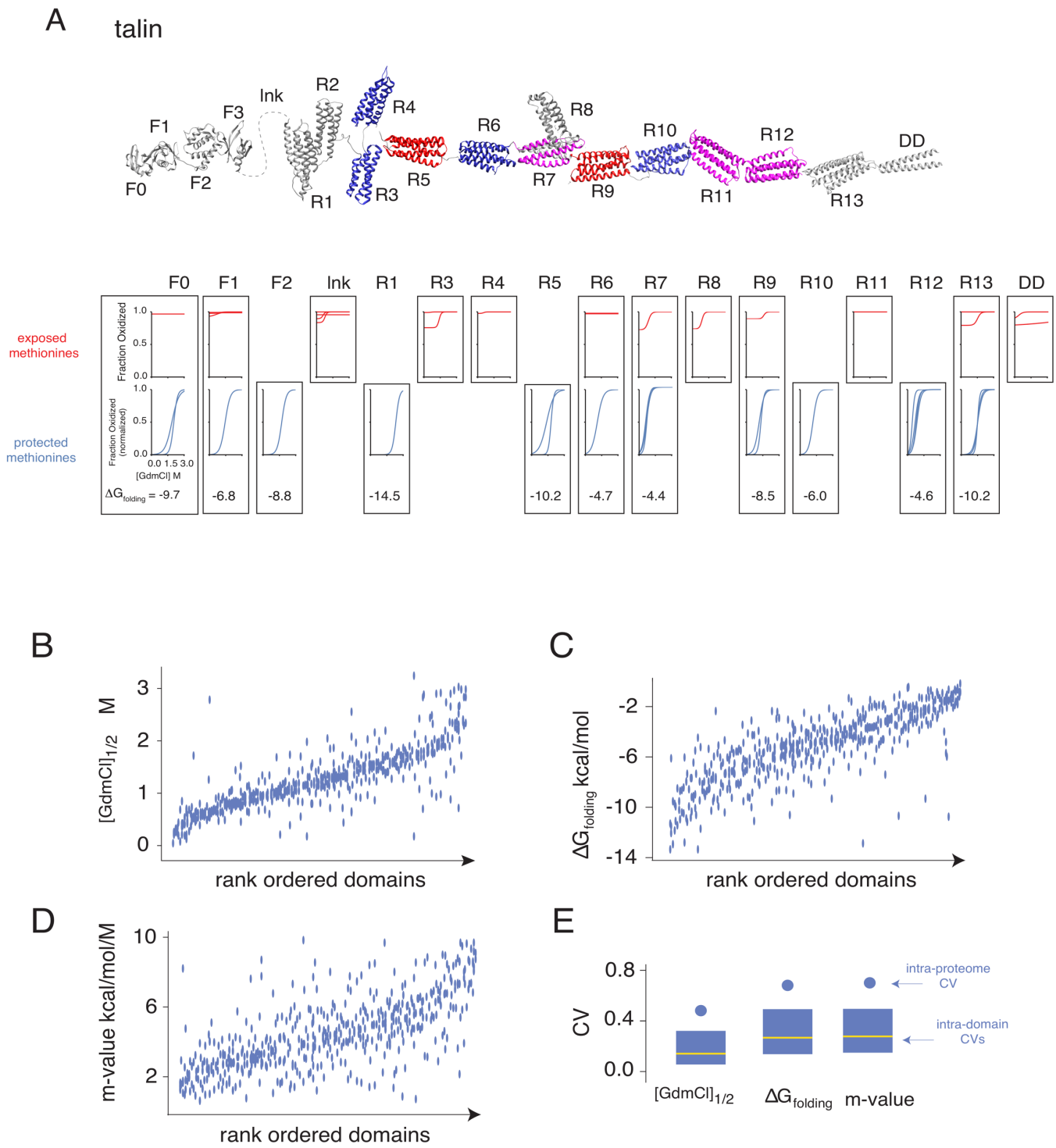
A
talin
F0
F1
F2
F3
lnk
R1
R2
R3
R4
R5
R6
R7
R8
R9
R10
R11
R12
R13
DD
exposed methionines
protected methionines
Fraction Oxidized
Fraction Oxidized (normalized)
[GdmCl] M
ΔG folding = -9.7
-6.8
-8.8
-14.5
-10.2
-4.7
-4.4
-8.5
-6.0
-4.6
-10.2
B
[GdmCl]1/2 M
rank ordered domains
C
ΔG folding kcal/mol
rank ordered domains
D
m-value kcal/mol/M
rank ordered domains
E
CV
intra-proteome CV
intra-domain CVs
[GdmCl]1/2
ΔG folding
m-value

Figure 6

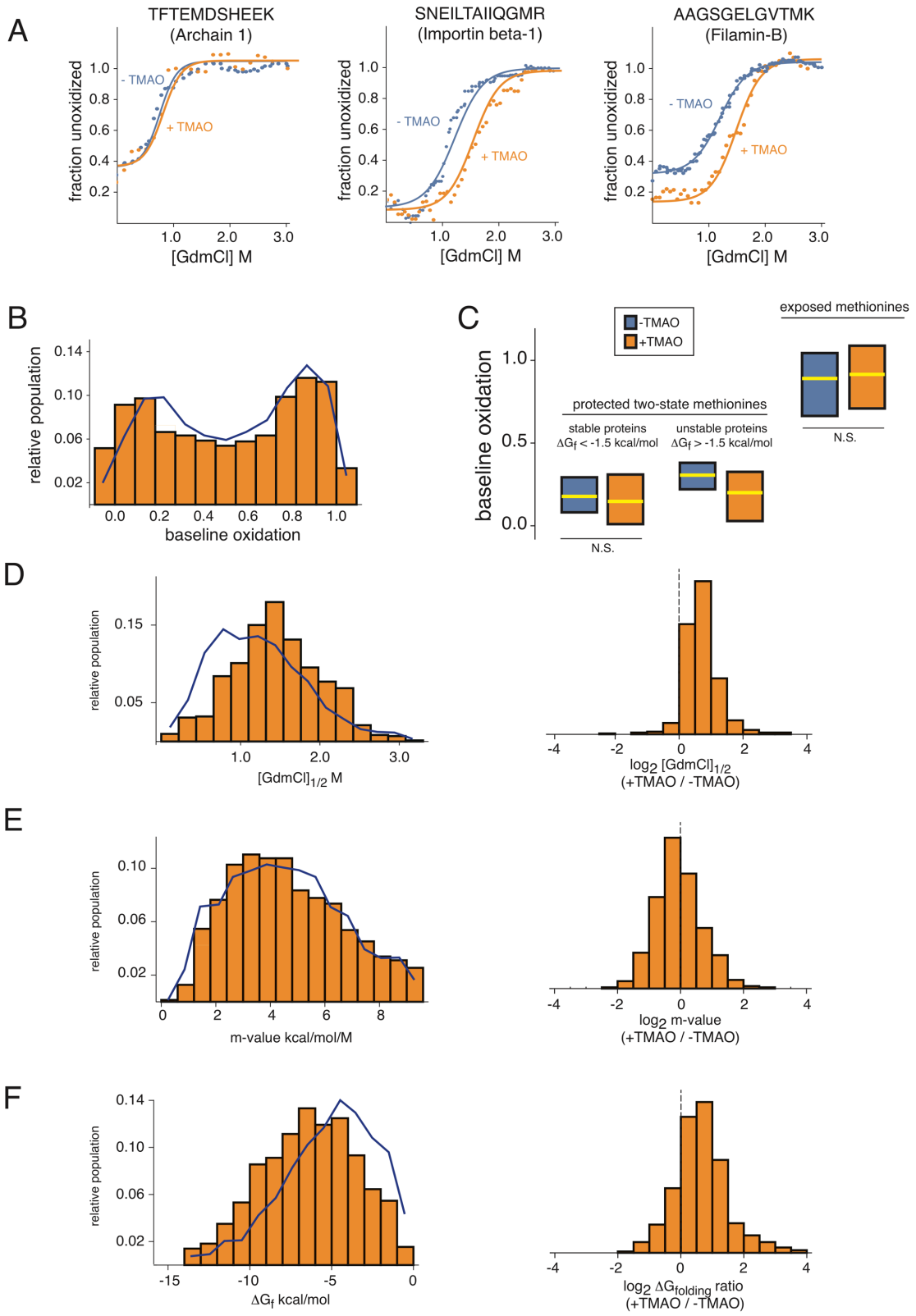
A
TFTEMDSHEEK
(Archain 1)
SNEILTAIIQGMR
(Importin beta-1)
AAGSGELGVTMK
(Filamin-B)
fraction unoxidized
- TMAO
+ TMAO
[GdmCl] M
B
relative population
baseline oxidation
C
-TMAO
+TMAO
baseline oxidation
exposed methionines
N.S.
protected two-state methionines
stable proteins
ΔGf < -1.5 kcal/mol
unstable proteins
ΔGf > -1.5 kcal/mol
N.S.
D
relative population
[GdmCl]1/2 M
log2 [GdmCl]1/2
(+TMAO / -TMAO)
E
relative population
m-value kcal/mol/M
log2 m-value
(+TMAO / -TMAO)
F
relative population
ΔGf kcal/mol
log2 ΔGfolding ratio
(+TMAO / -TMAO)

Figure 7

FIGURE LEGENDS

Figure 1. HR-SPROX as a tool for measuring protein stability. (A) Theoretical basis of SPROX. Methionine residues (white squares) are oxidized by H_2O_2 to form methionine sulfoxides (red squares). Methionine oxidation rates differ between folded and unfolded states. Thus, protein denaturation can be quantified by measuring the extent of oxidation across different denaturant concentrations at a constant oxidation time (dashed line). The resulting denaturation curves contain 4 categories of information (numbered 1-4): baseline oxidation, midpoint of denaturation ($[\text{denaturant}]_{1/2}$), m-value, and free energy of folding ($\Delta G_{folding}$ or ΔG_f). For two-state proteins, the latter two parameters can be determined by fitting the denaturation curve to an equation derived from the linear extrapolation model (LEM). (B) HR-SPROX workflow. Cells are lysed under native conditions and folded proteins (black ovals) are unfolded with increasing concentrations of GdmCl. Methionines are converted to methionine sulfoxides (red squares) by addition of H_2O_2. A control experiment lacking H_2O_2 is included and used as a normalization point. Extracts are digested into peptides and each sample (corresponding to a different denaturant concentration) is labeled with a unique tandem mass tag (TMT) and subsequently combined and analyzed by LC-MS/MS. Reporter ion intensities at the MS2 level are internally normalized to create denaturation curves, monitoring either the increase in methionine sulfoxide-containing peptides or the decrease in unoxidized methionine-containing peptides.

Figure 2. Validation of HR-SPROX by analysis of purified lysozyme (A) The structure of hen lysozyme (1DPX). Buried tryptophan residues analyzed by

fluorescence are colored in green, and the buried methionine residue analyzed by SPROX is colored in blue. (B) Denaturation curves obtained by intrinsic fluorescence (green) and SPROX (blue). The data were fit with Equation 1 to determine $\Delta G_{folding}$ and m-values.

Figure 3. Experimental design and example data for proteome-wide HR-SPROX analysis (A) Schematic representation of the experimental design for HR-SPROX analysis of the human fibroblast proteome indicating the replicates and denaturant concentrations used in the study. Each technical replicate consists of 3 complementary sets of GdmCl concentrations tagged with TMT 10-plex reagents. The data were combined after normalization, providing denaturation curves for 10,412 met-containing peptides. (B) Example HR-SPROX data for a protected methionine (highlighted in red) within a tryptic peptide in ADP-ribosylhydrolase (2FOZ). By combining a number of replicate measurements, detailed denaturation curves were obtained. Small black and red points indicate data obtained from methionine and methionine sulfoxide-containing peptides, respectively. The plots were smoothed by obtaining moving averages of the data (blue points) and fit by a two-state model (blue line) to determine $\Delta G_{folding}$, m-values, $[GdmCl]_{1/2}$ and baseline oxidation values. Also see Figures S1-3.

Figure 4. Global analysis of methionine baseline oxidation (A) The distribution of fractional methionine baseline oxidation levels within the analyzed proteome. Note that due to experimental noise, it is possible for $+H_2O_2$/0M GdmCl reporter ions to have a higher intensity than $+H_2O_2$/3M GdmCl reporter ions, resulting in measured oxidation levels greater than 1. (B) Relative baseline oxidation levels of peptides with different methionine-neighboring residues. Note that because the data consist of tryptic peptides,

sequences having lysine and arginine residues on the N-side of methionines are rare and not included in the analysis. (C-F) Comparison of baseline oxidation levels of methionines contained within different DSSP secondary structure elements (C), having different solvent accessible surface areas (D), having different disordered designations in accordance with MobiDB (E), and contained within proteins mapped to different gene ontologies (F). For all box plots, the medians are represented by yellow lines, and blue boxes denote interquartile ranges. The distributions being compared in box plots significantly differ from one another with p-values less than 0.001 using the Mann Whitney U test, with the exception of those grouped together under bars labeled "N.S." The histograms indicate the distributions of selected categories. Cross hatching indicates overlapping bars. Also see Figures S4-5.

Figure 5. Global analysis of thermodynamic folding parameters. (A) Quantified methionine-containing peptides were separated into one of three categories based on the observed characteristics of their denaturation curves: solvent exposed methionines (baseline oxidation>.5), protected two-state proteins (baseline oxidation<.5 and goodness-of-fit r^2 to two-state model>.9) and protected non-two-state proteins (baseline oxidation<.5 and r^2<.9). The scatter plots show averaged denaturation curves for example peptides in each category. The peptide used as an example of an exposed methionine is the MICAL oxidation site on actin, discussed in text. The pie chart indicates the number of peptides and proteins in each category. (B) Distributions of $[GdmCl]_{1/2}$, m-values and $\Delta G_{folding}$ measurements for two-state peptides. (C-D) Distributions of $[GdmCl]_{1/2}$ and $\Delta G_{folding}$ measurements for example gene ontology terms enriched in stable or unstable methionine-containing peptides. (E) The relationship

between protein stability ($\Delta G_{folding}$) and baseline methionine oxidation levels. See Figure 4 for description of box and bar plots. Also see Figure S6.

Figure 6. Inter- and intra-domain comparisons of thermodynamic folding parameters. (A) Talin is presented as an example of an analyzed multi-domain protein. The depicted structure is a composite of available structures for individual domains. The color coding indicates “weak” (blue), “intermediate” (pink) and “strong” (red) mechanical stabilities designated by Haining et al.[44] based on unfolding force magnitudes of domains in smAFM and steered molecular dynamics studies. Denaturation curves represent exposed (red) or protected (blue) methionine-containing peptides in different domains. For protected methionines, fractional oxidation measurements were normalized with respect to the native and denatured baselines. The reported $\Delta G_{folding}$ is the median of all protected methionines. (B-D) Global analysis of intra-domain variation. Using boundaries defined by the Pfam database, $[GdmCl]_{1/2}$ (B), $\Delta G_{folding}$ (C), and m-values (D) were assigned to specific domains. Measurements within all domains were rank ordered based on their median values. Peptide measurements mapped to a given domain are plotted on the y-axis for each rank-ordered domain represented on the x-axis. (E) The distributions of coefficients of variation (CV) of $[GdmCl]_{1/2}$, $\Delta G_{folding}$ and m-value measurements for different peptides within individual domains (intra-domain variation) compared to the CV of the measurements in the entire dataset (intra-proteome variation). See Figure 4 for description of box plots. The blue dots represent the median CV values for all analyzed peptides in the proteome.

Figure 7. The effect of the chemical chaperone TMAO on proteome stability (A) The effects of TMAO on denaturation curves of three example peptides mapped to different proteins. The data indicate that TMAO has variable effects on baseline oxidation levels and stabilities of different protein regions. (B) The distribution of relative methionine baseline oxidation levels within the analyzed proteome in the absence (blue lines, reproduced from Figure 4) and presence of 1 M TMAO (orange bars). (C) Impact of TMAO on baseline oxidation levels of exposed and protected proteins with different stabilities. (D-F) Impact of TMAO on distributions of $[GdmCl]_{1/2}$ (D), m-values (E) and $\Delta G_{folding}$ (F). The distributions of the measurements are compared in the absence (blue lines, reproduced from Figure 5) and presence of 1 M TMAO (orange bars), and also presented as $\log_2$ ratios of the measurements. See Figure 4 for description of box plots. Also see Figure S7.

TABLES

Table 1. Combined quantified proteome coverage of HR-SPROX analyses (-TMAO)

incorporated residue	unique peptides	unique proteins
met(unmodified)	5,719	1,977
met(ox)	9,350	2,977
met(unmodified) & met(ox)	4,565	1,745
met(unmodified) or met(ox)	10,412	3,158

REFERENCES

1. Henzler-Wildman, K. & Kern, D. Dynamic personalities of proteins. *Nature* **450**, 964-72 (2007).

2. Bryngelson, J.D., Onuchic, J.N., Socci, N.D. & Wolynes, P.G. Funnels, pathways, and the energy landscape of protein folding: a synthesis. *Proteins* **21**, 167-95 (1995).

3. Schellman, J.A. The thermodynamic stability of proteins. *Annu Rev Biophys Biophys Chem* **16**, 115-37 (1987).

4. Berlett, B.S. & Stadtman, E.R. Protein oxidation in aging, disease, and oxidative stress. *J Biol Chem* **272**, 20313-6 (1997).

5. Redler, R.L., Das, J., Diaz, R.J. & Dokholyan, N.V. Protein Destabilization as a Common Factor in Diverse Inherited Disorders. *J mol evol* **82**, 11-16 (2016).

6. Boopathy, S. et al. Structural basis for mutation-induced destabilization of profilin 1 in ALS. *Proc Natl Acad Sci U S A* **112**, 7984-9 (2015).

7. Smith, C.D. et al. Excess brain protein oxidation and enzyme dysfunction in normal aging and in Alzheimer disease. *Proc Natl Acad Sci U S A* **88**, 10540-3 (1991).

8. Dobson, C.M. Protein folding and misfolding. *Nature* **426**, 884-90 (2003).

9. Leuenberger, P. et al. Cell-wide analysis of protein thermal unfolding reveals determinants of thermostability. *Science* **355**(2017).

10. Oldfield, C.J. & Dunker, A.K. Intrinsically disordered proteins and intrinsically disordered protein regions. *Annu Rev Biochem* **83**, 553-84 (2014).

11. Pace, C.N., and J. Martin Scholtz. Measuring the conformational stability of a protein. *Protein structure: A practical approach* **2**, 299-321 (1997).

12. Krishna, M.M., Hoang, L., Lin, Y. & Englander, S.W. Hydrogen exchange methods to study protein folding. *Methods* **34**, 51-64 (2004).

13. Ghaemmaghami, S., Fitzgerald, M.C. & Oas, T.G. A quantitative, high-throughput screen for protein stability. *Proceedings of the National Academy of Sciences of the United States of America* **97**, 8296-8301 (2000).

14. Kiselar, J. & Chance, M.R. High-Resolution Hydroxyl Radical Protein Footprinting: Biophysics Tool for Drug Discovery. *Annu Rev Biophys* (2018).

15. Park, C. & Marqusee, S. Pulse proteolysis: a simple method for quantitative determination of protein stability and ligand binding. *Nat Methods* **2**, 207-12 (2005).

16. Feng, Y. et al. Global analysis of protein structural changes in complex proteomes. *Nat Biotechnol* **32**, 1036-44 (2014).

17. Savitski, M.M. et al. Tracking cancer drugs in living cells by thermal profiling of the proteome. *Science* **346**, 1255784 (2014).

18. Becher, I. et al. Pervasive Protein Thermal Stability Variation during the Cell Cycle. *Cell* **173**, 1495-1507 e18 (2018).

19. West, G.M., Tang, L. & Fitzgerald, M.C. Thermodynamic Analysis of Protein Stability and Ligand Binding Using a Chemical Modification- and Mass Spectrometry-Based Strategy. *Analytical Chemistry* **80**, 4175-4185 (2008).

20. West, G.M. et al. Quantitative proteomics approach for identifying protein-drug interactions in complex mixtures using protein stability measurements. *Proc Natl Acad Sci U S A* **107**, 9078-82 (2010).

21. Xu, Y., Wallace, M.A. & Fitzgerald, M.C. Thermodynamic Analysis of the Geldanamycin-Hsp90 Interaction in a Whole Cell Lysate Using a Mass Spectrometry-Based Proteomics Approach. *J Am Soc Mass Spectrom* **27**, 1670-6 (2016).

22. Reeg, S. & Grune, T. Protein Oxidation in Aging: Does It Play a Role in Aging Progression? *Antioxid Redox Signal* **23**, 239-55 (2015).

23. Zull, J.E. & Chuang, J. Characterization of parathyroid hormone fragments produced by cathepsin D. *J Biol Chem* **260**, 1608-13 (1985).

24. Lam, X.M., Yang, J.Y. & Cleland, J.L. Antioxidants for prevention of methionine oxidation in recombinant monoclonal antibody HER2. *J Pharm Sci* **86**, 1250-5 (1997).

25. Xu, K., Uversky, V.N. & Xue, B. Local flexibility facilitates oxidization of buried methionine residues. *Protein Pept Lett* **19**, 688-97 (2012).

26. Pace, C.N. Determination and analysis of urea and guanidine hydrochloride denaturation curves. *Methods Enzymol* **131**, 266-80 (1986).

27. Myers, J.K., Pace, C.N. & Scholtz, J.M. Denaturant m values and heat capacity changes: relation to changes in accessible surface areas of protein unfolding. *Protein Sci* **4**, 2138-48 (1995).

28. Ahmad, F. & Bigelow, C.C. Estimation of the free energy of stabilization of ribonuclease A, lysozyme, alpha-lactalbumin, and myoglobin. *J Biol Chem* **257**, 12935-8 (1982).

29. Bodnar, A.G. et al. Extension of life-span by introduction of telomerase into normal human cells. *Science* **279**, 349-52 (1998).

30. Deutsch, E.W. et al. The ProteomeXchange consortium in 2017: supporting the cultural change in proteomics public data deposition. *Nucleic Acids Res* **45**, D1100-D1106 (2017).

31. Aledo, J.C., Canton, F.R. & Veredas, F.J. Sulphur Atoms from Methionines Interacting with Aromatic Residues Are Less Prone to Oxidation. *Sci Rep* **5**, 16955 (2015).

32. Kabsch, W. & Sander, C. Dictionary of protein secondary structure: pattern recognition of hydrogen-bonded and geometrical features. *Biopolymers* **22**, 2577-637 (1983).

33. Humphrey, W., Dalke, A. & Schulten, K. VMD: visual molecular dynamics. *J Mol Graph* **14**, 33-8, 27-8 (1996).

34. Romero, P. et al. Sequence complexity of disordered protein. *Proteins* **42**, 38-48 (2001).

35. Piovesan, D. et al. MobiDB 3.0: more annotations for intrinsic disorder, conformational diversity and interactions in proteins. *Nucleic Acids Res* **46**, D471-D476 (2018).

36. Hung, R.J. et al. Mical links semaphorins to F-actin disassembly. *Nature* **463**, 823-7 (2010).

37. Hung, R.J., Pak, C.W. & Terman, J.R. Direct redox regulation of F-actin assembly and disassembly by Mical. *Science* **334**, 1710-3 (2011).

38. Manta, B. & Gladyshev, V.N. Regulated methionine oxidation by monooxygenases. *Free Radic Biol Med* **109**, 141-155 (2017).

39. Pace, C.N. The stability of globular proteins. *CRC Crit Rev Biochem* **3**, 1-43 (1975).

40. Ghosh, K. & Dill, K. Cellular proteomes have broad distributions of protein stability. *Biophys J* **99**, 3996-4002 (2010).

41. Bohley, P. & Seglen, P.O. Proteases and proteolysis in the lysosome. *Experientia* **48**, 151-7 (1992).

42. Patel, A. et al. ATP as a biological hydrotrope. *Science* **356**, 753-756 (2017).

43. Batey, S., Nickson, A.A. & Clarke, J. Studying the folding of multidomain proteins. *HFSP J* **2**, 365-77 (2008).

44. Haining, A.W., von Essen, M., Attwood, S.J., Hytonen, V.P. & Del Rio Hernandez, A. All Subdomains of the Talin Rod Are Mechanically Vulnerable and May Contribute To Cellular Mechanosensing. *ACS Nano* **10**, 6648-58 (2016).

45. del Rio, A. et al. Stretching single talin rod molecules activates vinculin binding. *Science* **323**, 638-41 (2009).

46. Yao, M. et al. Mechanical activation of vinculin binding to talin locks talin in an unfolded conformation. *Sci Rep* **4**, 4610 (2014).

47. Finn, R.D. et al. The Pfam protein families database: towards a more sustainable future. *Nucleic Acids Res* **44**, D279-85 (2016).

48. Yancey, P.H., Clark, M.E., Hand, S.C., Bowlus, R.D. & Somero, G.N. Living with water stress: evolution of osmolyte systems. *Science* **217**, 1214-22 (1982).

49. Ma, J., Pazos, I.M. & Gai, F. Microscopic insights into the protein-stabilizing effect of trimethylamine N-oxide (TMAO). *Proc Natl Acad Sci U S A* **111**, 8476-81 (2014).

50. Baskakov, I. & Bolen, D.W. Forcing thermodynamically unfolded proteins to fold. *J Biol Chem* **273**, 4831-4 (1998).

51. Mello, C.C. & Barrick, D. Measuring the stability of partly folded proteins using TMAO. *Protein Sci* **12**, 1522-9 (2003).

52. Ganguly, P., Boserman, P., van der Vegt, N.F.A. & Shea, J.E. Trimethylamine N-oxide Counteracts Urea Denaturation by Inhibiting Protein-Urea Preferential Interaction. *J Am Chem Soc* **140**, 483-492 (2018).

53. Levine, R.L., Mosoni, L., Berlett, B.S. & Stadtman, E.R. Methionine residues as endogenous antioxidants in proteins. *Proc Natl Acad Sci U S A* **93**, 15036-40 (1996).

54. Cabreiro, F., Picot, C.R., Friguet, B. & Petropoulos, I. Methionine sulfoxide reductases: relevance to aging and protection against oxidative stress. *Ann N Y Acad Sci* **1067**, 37-44 (2006).

55. Weissbach, H. et al. Peptide methionine sulfoxide reductase: structure, mechanism of action, and biological function. *Arch Biochem Biophys* **397**, 172-8 (2002).

56. Yancey, P.H., Blake, W.R. & Conley, J. Unusual organic osmolytes in deep-sea animals: adaptations to hydrostatic pressure and other perturbants. *Comp Biochem Physiol A Mol Integr Physiol* **133**, 667-76 (2002).

57. Zou, Q., Bennion, B.J., Daggett, V. & Murphy, K.P. The molecular mechanism of stabilization of proteins by TMAO and its ability to counteract the effects of urea. *J Am Chem Soc* **124**, 1192-202 (2002).

58. McDowell, G.S., Gaun, A. & Steen, H. iFASP: combining isobaric mass tagging with filter-aided sample preparation. *J Proteome Res* **12**, 3809-12 (2013).

59. Cox, J. & Mann, M. MaxQuant enables high peptide identification rates, individualized p.p.b.-range mass accuracies and proteome-wide protein quantification. *Nat Biotechnol* **26**, 1367-72 (2008).

60. Velankar, S. et al. SIFTS: Structure Integration with Function, Taxonomy and Sequences resource. *Nucleic Acids Res* **41**, D483-9 (2013).

61. Burley, S.K. et al. Protein Data Bank (PDB): The Single Global Macromolecular Structure Archive. *Methods Mol Biol* **1607**, 627-641 (2017).

62. The Gene Ontology, C. Expansion of the Gene Ontology knowledgebase and resources. *Nucleic Acids Res* **45**, D331-D338 (2017).

63. Supek, F., Bosnjak, M., Skunca, N. & Smuc, T. REVIGO summarizes and visualizes long lists of gene ontology terms. *PLoS One* **6**, e21800 (2011).

SUPPLEMENTARY INFORMATION

METHODS

Cell culture.

Human diploid fibroblasts expressing telomerase (HCA2-hTert)[29] were cultured at 37°C, 5% CO_2, in Eagle's minimum essential medium (EMEM) supplemented with 15% fetal bovine serum (FBS), 100 U/mL penicillin and 100 U/mL streptomycin. Cells were grown to 100% confluency and maintained for at least 4 days to ensure they reached a quiescent state. Cells were harvested, washed twice with phosphate buffered saline (PBS), and the pellets were stored at -80°C until analysis.

Preparation of stock solutions.

Native lysis buffer was prepared by dissolving 1 Pierce EDTA-free protease inhibitor mini tablet in 10 mL of a filtered 20 mM sodium phosphate buffer (pH 7.4) with 50 mM NaCl (Fisher). All GdmCl stocks were prepared volumetrically by mixing ratios of a filtered 7 M stock solution of ultrapure GdmCl (Sigma-Aldrich) dissolved in 20 mM sodium phosphate buffer (pH 7.4) with filtered phosphate buffer only. All GdmCl stocks were kept at room temperature (RT) for no longer than 3 months. Urea-containing buffers were prepared fresh on the day of analysis and made volumetrically from high purity (≥99.5%) urea pellets (Sigma-Aldrich) for a final concentration of 8 M urea in 0.1 M triethylammonium bicarbonate (TEAB) buffer (pH 8.5). tris(2-carboxyethyl)phosphine (TCEP) quenching buffers were prepared volumetrically from TCEP hydrochloride

(Sigma-Aldrich), adjusted to neutral pH with concentrated NaOH (Fisher), and diluted to 0.5 M (of note, for samples 1-10 the pH was adjusted only by resuspending TCEP at 0.5M in TEAB buffer). Iodoacetamide (IAA) buffer for protein alkylation was prepared immediately before use from high purity IAA (Sigma) dissolved in urea buffer. For all buffers, MS-grade water (Thermo Scientific) was used as a diluent.

Protein extraction.

On the day of analysis, cell pellets were resuspended in native lysis buffer at 50 µL per 10^6 cells. Lysis was accomplished by repeated passage through a 16-gauge sterile syringe, resting on ice, after which the samples were centrifuged for 10 min at 13000xg while at 4°C, and the supernatants collected. Protein concentration was subsequently measured using a BCA assay and samples were diluted to a final concentration of 5 mg/mL, with the exception of experiments 10-15 which were diluted to 2 mg/mL.

Sample preparation and TMT tagging.

Protein extracts were aliquoted out in 25 µL portions into 30 wells of a 96-deepwell polypropylene microplate (Fisher Scientific). 3 wells were kept as a control (no H_2O_2, no GdmCl) for measuring background levels of methionine oxidation, and the remaining wells were split into 3 complementary sets of denaturant-containing buffers such that their final concentrations ranged between 0-3 M GdmCl (see Figure 3A), allowed to equilibrate for 1 hr at RT, and oxidized with 3% H_2O_2 for 1 min. Oxidation was quenched using a four-fold molar excess of TCEP, and protein was purified using 30-kDa centrifugal filters (Millipore Sigma) in a modified iFASP procedure[58]. During this process, proteins were fully denatured using 8 M urea, disulfide bonds were reduced

with 5 mM TCEP in urea buffer for 1 hr at RT, and proteins were alkylated by incubating with 50 mM IAA for 20 min at RT in darkness. After washing out the denaturant, proteins were digested with trypsin protease (Pierce) at a 1:100 ratio (g protein/g trypsin), incubating overnight at 37°C in a wet bath. Trypsin was quenched by adding formic acid (Fisher Scientific) to a final concentration of 1%, after which samples were dried down and 25 μg (10 μg for experiments 10-15) of digest was resuspended in 0.1 M TEAB for labeling using TMT 10-plex reagents (Thermo Scientific). TMT labeling was accomplished using 0.2 mg of TMT 10plex reagents (Thermo Scientific) suspended in acetonitrile (Thermo Scientific) and incubating for 1 hr at RT. TMT labeling was quenched using 5% hydroxylamine (Fisher Scientific), incubating for 15 min at RT. For each of the TMT sets, 5 μg portions of labeled digest were combined and dried down.

Peptide fractionation by spin column.

To increase coverage, samples were fractionated using lab-made C18 spin columns. Columns were first conditioned using acetonitrile (ACN) and 100 mM ammonium formate (AF) buffer (pH 10). Samples were resuspended in 50 μL of AF buffer and added to the columns. After washing the columns with 5% ACN in AF buffer, samples were eluted with 10%, 12.5%, 15%, 17.5%, 20%, 22.5%, 25%, and then 50% ACN (in AF buffer). Eluent fractions were then dried down and resuspended in MS-grade 0.1% trifluoroacetic acid (TFA) in water (Thermo Scientific) at a concentration of 0.25 mg/ml for LC-MS/MS analysis.

Proteome stability in the presence of TMAO.

For these analyses, protein extracts were prepared at a concentration of ~5 mg/ml, using the method described above. On the day of analysis, a concentrated TMAO stock solution was prepared from TMAO dihydrate dissolved in 20 mM sodium phosphate buffer (pH 7.4). Immediately prior to incubation in GdmCl, samples were mixed with the TMAO stock solution such that the final concentration of TMAO was 1 M. Samples were then processed and fractionated as above.

Mass spectrometric analysis.

Analyses of -TMAO experiments 1-6 and +TMAO experiments 1-3 (see Figure 3A, S7A) were conducted on a Q Exactive Plus instrument, and the remainder of the experiments were conducted on a Fusion Lumos Tribrid instrument as described below.

For Fusion Lumos LC-MS/MS analysis, peptides were injected onto a homemade 30 cm C18 column with 1.8 um beads (Sepax), with an Easy nLC-1200 HPLC (Thermo Fisher), connected to a Fusion Lumos Tribrid mass spectrometer (Thermo Fisher). Solvent A was 0.1% formic acid in water, while solvent B was 0.1% formic acid in 80% ACN. Ions were introduced to the mass spectrometer using a Nanospray Flex source operating at 2 kV. The gradient began at 3% B and held for 2 min, increased to 10% B over 7 min, increased to 38% B over 94 min, then ramped up to 90% B in 5 min and was held for 3 min, before returning to starting conditions in 2 min and re-equilibrating for 7 min, for a total run time of 120 min. The Fusion Lumos was operated in data-dependent mode, with both MS1 and MS2 scans acquired in the Orbitrap. The cycle time was set to 3 seconds. Monoisotopic Precursor Selection (MIPS) was set to Peptide. The full scan was done over a range of 400-1500 m/z, with a resolution of

120,000 at m/z of 200, an AGC target of 4e5, and a maximum injection time of 50 ms. Peptides with a charge state between 2-5 were picked for fragmentation. Precursor ions were fragmented by higher-energy collisional dissociation (HCD) using a collision energy of 36% and an isolation width of 0.7 m/z. MS2 scans were collected with a resolution of 50,000, a maximum injection time of 105 ms, and an AGC setting of 1e5. Dynamic exclusion was set to 45 seconds.

For Q Exactive Plus LC-MS/MS analysis, peptides were injected onto a homemade 30 cm C18 column with 1.8 um beads (Sepax), with an Easy nLC-1000 HPLC (Thermo Fisher), connected to a Q Exactive Plus mass spectrometer (Thermo Fisher). Solvent A was 0.1% formic acid in water, while solvent B was 0.1% formic acid in ACN. Ions were introduced to the mass spectrometer using a Nanospray Flex source operating at 2 kV. The gradient began at 6% B and held for 2 minutes, increased to 30% B over 85 min, increased to 50% B over 10 min, then ramped up to 70% B in 4 min and was held for 5 min, before returning to starting conditions in 4 min and re-equilibrating for 10 min, for a total run time of 120 min. The Q Exactive Plus was operated in data-dependent mode, with a full scan followed by 10 MS/MS scans. The full scan was done over a range of 400-1700 m/z, with a resolution of 70,000 at m/z of 200, an AGC target of 1e6, and a maximum injection time of 50 ms. Peptides with a charge state between 2-5 were picked for fragmentation. Precursor ions were fragmented by higher-energy collisional dissociation (HCD) using a collision energy of 35 and an isolation width of 1.0 m/z, with an offset of 0.3 m/z. MS2 scans were collected with a resolution of 35,000, a maximum injection time of 120 ms, and an AGC setting of 1e5. The fixed first mass for the MS2

scans was set to 120 m/z to ensure TMT reporter ions were always collected. Dynamic exclusion was set to 25 seconds.

Thermodynamic stability measurements of lysozyme.

To measure intrinsic fluorescence, a solution of 10 μM chicken egg white lysozyme (Fisher) was prepared in 20 mM sodium phosphate buffer (pH 7.4) containing either 0 M or 7 M GdmCl. Denaturation was performed at the final concentrations of 0, 0.3, 0.6, 0.9, 1.2, 1.5, 1.8, 2.1, 2.4, 2.7, 3.0, 3.2, 3.4, 3.6, 3.8, 4.0, 4.2, 4.4, 4.6, 4.8, 5.0, 5.2, 5.4, 5.6, 5.8, 6.0, 6.2, 6.4, 6.6, 6.8, or 7.0 M GdmCl. Samples were then aliquoted out in triplicate in a black 96-well (Evergreen) microplate, incubating for 4 hr at RT. Samples were then analyzed on a SpectraMax M2 spectrophotometer, with a 280 nm excitation wavelength and emission wavelengths measured from 300-460 nm in steps of 5 nm. The relative fluorescence emission data at 360 nm was subsequently used to measure the fraction of unfolded protein.

For HR-SPROX analysis, lysozyme was dissolved at a concentration of 2 mg/mL in 20 mM sodium phosphate buffer (pH 7.4) and prepared using the method above, with the following modifications: Final GdmCl concentrations were 0, 0.3, 0.6, 0.9, 1.3, 1.6, 2, 2.4, 2.6, 2.8, 3, 3.2, 3.4, 3.6, 3.8, 4.0, 4.2, 4.4, 4.6, 4.8, 5, 5.5, 6, and 7 M. In place of fractionation, lysozyme samples were desalted using lab-made C18 spin columns. Columns were first conditioned using 50% ACN in 0.1% TFA, and 0.1% TFA. Samples were resuspended in 50 μL of 0.1% TFA and added to the columns. After washing the columns with 0.1% TFA, samples were eluted with 50% ACN in 0.1% TFA.

Database searches and quantitation.

All MS2 data were searched against the *H. sapiens* UniProt database (20,975 entries, downloaded 6/18/2017) using the integrated Andromeda search engine with MaxQuant software[59]. The searches included the TMT10-plex labels as fixed modifications and methionine oxidation as variable modifications and allowed for up to two missed cleavages with maximum false discovery rate (FDR) thresholds of 1%. For searches described in Figure S1, additional variable modifications were included as described. The complete parameter settings for MaxQuant searches, and the search results are provided in Supplementary Tables 1-3.

Measurement of $[GdmCl]_{1/2}$, $\Delta G_{folding}$, m-values and baseline oxidation levels.

Subsequent analyses of MaxQuant search results and quantitations were conducted with scripts written in house using Mathematica (Wolfram). MaxQuant searches produced reporter ion intensities for 15 different TMT 10-plex experiments for -TMAO analyses and 6 for +TMAO experiments, with each tag corresponding to a different GdmCl concentration within a methionine oxidation denaturation curve. Reporter ion intensities within each 10-plex experiment were normalized with respect to one another using the median intensities of non-methionine-containing peptides. For each 10-plex experiment, the data for methionine-sulfoxide-containing (Met-O) peptides were converted to fraction oxidized by using the intensities of no-H_2O_2/0M GdmCl and highest concentration GdmCl data-points as initial and final baselines, respectively. For methionine-containing (Met) peptides, the inverse fractions were obtained by reversing the baselines. For sequences containing more than one methionine, the fully oxidized and fully unoxidized peptides were analyzed as Met-O and Met variants, respectively. Initially, the amplitudes and midpoints of denaturation curves ($[GdmCl]_{1/2}$) for Met and

Met-O containing peptides within each 10-plex experiments was measured by least squares fitting of each curve with the following sigmoidal equation:

$$\text{fraction oxidized} = (1 - \text{amplitude}) + \frac{\text{amplitude}}{1+(\frac{[\text{GdmCl}]}{[\text{GdmCl}]_{1/2}})^{-\text{H}}} \quad (1)$$

Where H is the largest absolute value of the slope of the curve. The amplitude and midpoints of peptides shared between different TMT 10-plex experiments were shown to be generally well correlated (Figure S2). The fraction oxidized data for each peptide contained in different TMT 10-plex experiments were merged by using the no-H_2O_2/0M GdmCl, H_2O_2/0M GdmCl and H_2O_2/highest GdmCl concentration as shared anchor points. The merged data (containing up to 300 individual [GdmCl] for each peptide (Figure S3)) were then fit to equation 12 (see below) by least squares fitting and $[\text{GdmCl}]_{1/2}$, $\Delta G_{folding}$, m-values and baseline oxidation levels were determined. The two-state model is formally described below. Measured parameters for each peptide are provided in Supplementary Table 4.

Two-state model.

We start by considering a two-state protein with a single methionine that can exist in completely folded or completely unfolded states:

$$U \xleftrightarrow{K_{folding}} F \quad (2)$$

$K_{folding}$ is the folding equilibrium constant and is related to the thermodynamic stability ($\Delta G_{folding}$) by the following relationship:

$$K_{folding} = e^{-\frac{\Delta G_{folding}}{RT}} \quad (3)$$

Where R is the gas constant, and T is the absolute temperature in Kelvin. Using the linear extrapolation model (LEM), the apparent free energy of folding changes linearly with respect to denaturant concentration ([D]):

$$\Delta G_{apparent}(\mathrm{D}) = \Delta G_{folding} + \mathrm{m}[\mathrm{D}] \quad (4)$$

Where $\Delta G_{apparent}$ is the free energy measured at a given concentration of denaturant, $\Delta G_{folding}$ is the free energy in absence of denaturant, and m is the dependence of $\Delta G_{apparent}$ on denaturant concentration measured as the slope of the $\Delta G_{apparent}$ vs. [D] line. Thus, $K_{folding}$ at any given denaturant concentration can be described in terms of the apparent $\Delta G_{folding}$:

$$K_{folding}(\mathrm{D}) = e^{-\frac{(\Delta G_{folding} + m[D])}{RT}} \quad (5)$$

The rate of methionine oxidation will differ depending on whether the protein is in a folded or unfolded state. We refer to the pseudo-first order rate constants of oxidation within the folded or unfolded states as k_{ox}^{U} and k_{ox}^{F}, respectively. Thus, assuming first order kinetics, the fraction of the oxidized proteins within each state as a function of time can be defined as:

$$f_{ox}^{U}(t) = 1 - e^{-k_{ox}^{U} * t} \quad (6)$$

$$f_{ox}^{F}(t) = 1 - e^{-k_{ox}^{F} * t} \quad (7)$$

For a two-state protein, its conformational population will be divided into folded and unfolded fractions (f_F *and* f_U), in accordance to $K_{folding}$, which is a function of [D] as shown in equation 4:

$$f_U(\mathrm{D}) = \frac{1}{K_{folding}(\mathrm{D})+1} \tag{8}$$

$$f_F(\mathrm{D}) = \frac{K_{folding}(D)}{K_{folding}(\mathrm{D})+1} \tag{9}$$

And the overall fractional oxidation of the protein at a given time and denaturant concentration can be approximated by the following equation:

$$F_{ox}\,(t, D) = f_U(D) * f_{ox}^{U}\,(t) + f_F(D) * f_{ox}^{F}\,(t) \tag{10}$$

Note that equation 10 is making the assumption that the protein is pre-equilibrated between folded and unfolded populations - each having its own rate of oxidation. This model assumes that during the short H_2O_2 pulse, there is not sufficient time for a significant fraction of the folded population to convert to unfolded conformations and then oxidize. We can normalize the overall fractional oxidation with respect to the initial and final baselines (when the protein is fully folded or unfolded, respectively):

$$Normalized\ F_{ox}\,(t, [D]) = \frac{f_{ox}\,(t,D) - f_{ox}^{U}\,(t)}{f_{ox}^{F}\,(t) - f_{ox}^{U}\,(t)} \tag{11}$$

Substituting with equations 8 and 9, the equation simplifies to:

$$Normalized\ F_{ox}\,(D) = \frac{K_{folding}(D)}{K_{folding}(\mathrm{D})+1} = \frac{1}{1+e^{-(\Delta G_{folding}+m[D])/RT)}} \tag{12}$$

Note that while F_{ox} is a function of denaturant concentration, time, and the rate constants for oxidation for both the folded and unfolded states, $Normalized\ F_{ox}$ is solely a function of $K_{folding}$ (and thus $\Delta G_{folding}$, m, and $[D]$), and is not dependent on time and the rate constants for oxidation. This equation differs from the SPROX equation described by West et al. (equation 2 in [19]) due to the approximation implied in equation 10. However, under conditions where the oxidation time is short relative to the rate of methionine oxidation (as is the case in our experiments), these two equations are equivalent. As the conditions of SPROX experiments deviate from this approximation (e.g. longer pulse times or higher H_2O_2 concentrations), equation 12 will underestimate $\Delta G_{folding}$ values.

Analysis of neighboring residue effects on baseline oxidation.

Combined peptide data were binned based on the identities of the residues located at -3, -2, -1, +1, +2 and +3 positions in the primary sequence relative to methionine. Sequences containing more than one methionine were excluded in this analysis. Median baseline oxidation levels for each bin were measured, excluding far outliers (>2 SDs). Since tryptic peptides contain lysines and arginines at their carboxyl termini, -1, -2 and -3 bins for these two amino acids only contained a few mis-cleaved peptides and were excluded in this analysis.

Analysis of correlation between secondary structure and baseline oxidation.

Mappings of UniProt accessions to protein data bank (PDB) structures were obtained from the Structure Integration with Function, Taxonomy and Sequence (SIFTS) database (downloaded August 2018)[60]. DSSP secondary structure assignments were

obtained from the PDB (downloaded August 2018). Using this data, 2,526 methionines in our dataset were mapped to DSSP secondary structures (Supplementary Table 5). For each secondary structure, the baseline oxidation levels for the corresponding methionines were collected. The selected peptides were limited to those for which more than two independent data points were collected for measurement of fractional oxidation. The distribution and median of the peptide measurements were analyzed, excluding outliers (>2 SDs). In cases were multiple structures and DSSP assignments were available for a given methionine, the measurements corresponding to that methionine were included for all matched secondary structures.

Analysis of correlation between solvent accessibility and baseline oxidation.

UniProt accessions were mapped to PDB structures as above. For each mapped methionine, solvent accessible surface areas (SASA) were calculated from the associated PDB structures using the visualizing molecular dynamics (VMD) family of algorithms. For each structure, the coordinates of sulfur atoms belonging to methionines were found and analyzed for solvent accessibility using VMD's *atomselect* and *sasa* commands, respectively. Solvent accessibility calculations were conducted using a probe radius of 1.4 angstroms and restricted to the space not occupied by another atom. A subset of PDB files were excluded from the analysis due to substitution of methionine with selenomethione. In cases where multiple structures were mapped to a methionine, the median solvent accessible surface area was assigned to that methionine. Using this approach, we determined SASA values for 1,307 methionines in our dataset for which more than two independent data points were collected for measurement of fractional oxidation (Supplementary Table 5). Methionine baseline

oxidation levels for specific ranges of SASA were collected and the distribution and median of the measurements were analyzed, excluding outliers (>2 SDs).

Assignment of intrinsically disordered proteins (IDPs).

A database of disordered protein regions was obtained from MobiDB3.0[35]. Sequences classified as “derived”, in which disorder was determined based on a number of different feature characteristics of the PDB structures[61], were collected and mapped to 2,896 methionines in our dataset for which more than two independent data points were collected for measurement of fractional oxidation (Supplementary Table 5). Assignments in MobiDB are divided into “disordered” and “conflict” based on whether a consensus regarding their annotation exists using different guidelines for assignment of disorder[35]. The distribution and median of the baseline oxidation levels for methionines mapped to each category was determined, excluding outliers (>2 SDs).

Gene ontology (GO) analyses.

Mappings of GO terms to UniProt accessions, and their relational hierarchies were obtained from the gene ontology database (downloaded June 2018)[62]. For all proteins mapped to a given GO term, all methionine baseline oxidation levels, [GdmCl]1/2 and $\Delta G_{folding}$, values were collected. The p-values for differences between the distribution of these values for a given GO term, in comparison to the entire dataset were determined using the Mann-Whitney U test. GO terms having p-values less that 10^{-6} for fractional oxidation and less than 10^{-3} for $[GdmCl]_{1/2}$, m-value and $\Delta G_{folding}$ were identified for each parameter (Supplementary Table 6) and their connectivity was visualized using the program ReviGO[63] after excluding highly redundant terms (Figures S5-S6). For a

selection of terms with the most significant p-values, the distribution and median of the parameters were compared after excluding outliers (>2 SDs) (Figures 4,5).

Analyses of intra-domain variability.

Domain definitions and sequence boundaries were downloaded from the Pfam database (version 31.0, downloaded June 2018)[47]. A total of 1,055 methionine-containing peptides for which $[GdmCl]_{1/2}$,$\Delta G_{folding}$ and m-values were measured were mapped to 484 different Pfam domains (Supplementary Table 5). In analyzing the intra-domain distribution and CVs of these three parameters (e.g. Figure 6), only domains with more than one mapped methionine were considered.

Data and software availability

All analyzed data and measurements can be found in supplemental data files. The raw and processed MS proteomics data have been deposited to the ProteomeXchange Consortium via the PRIDE partner repository with the dataset identifier PXD011456.

Supplementary Figures

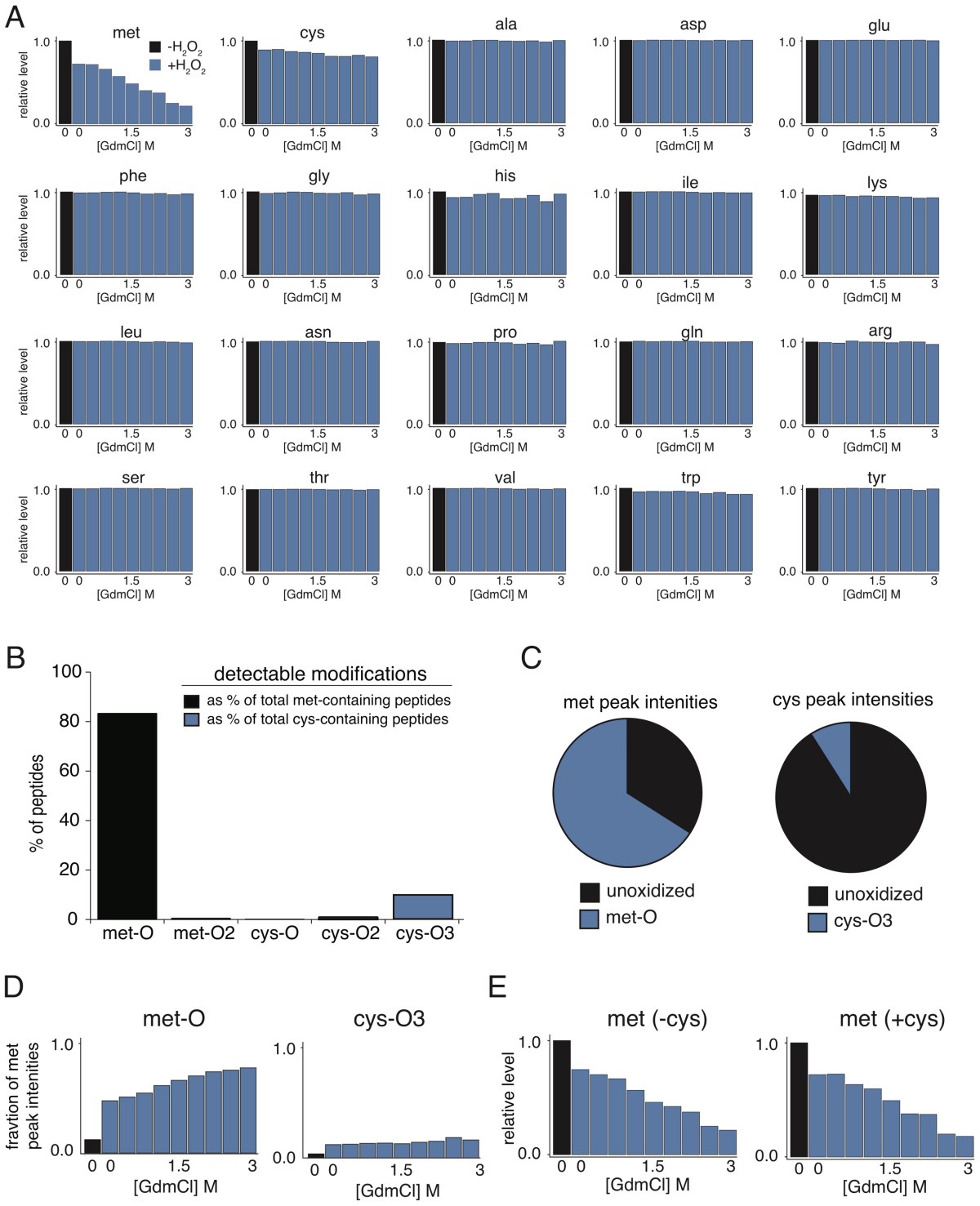

Figure S1

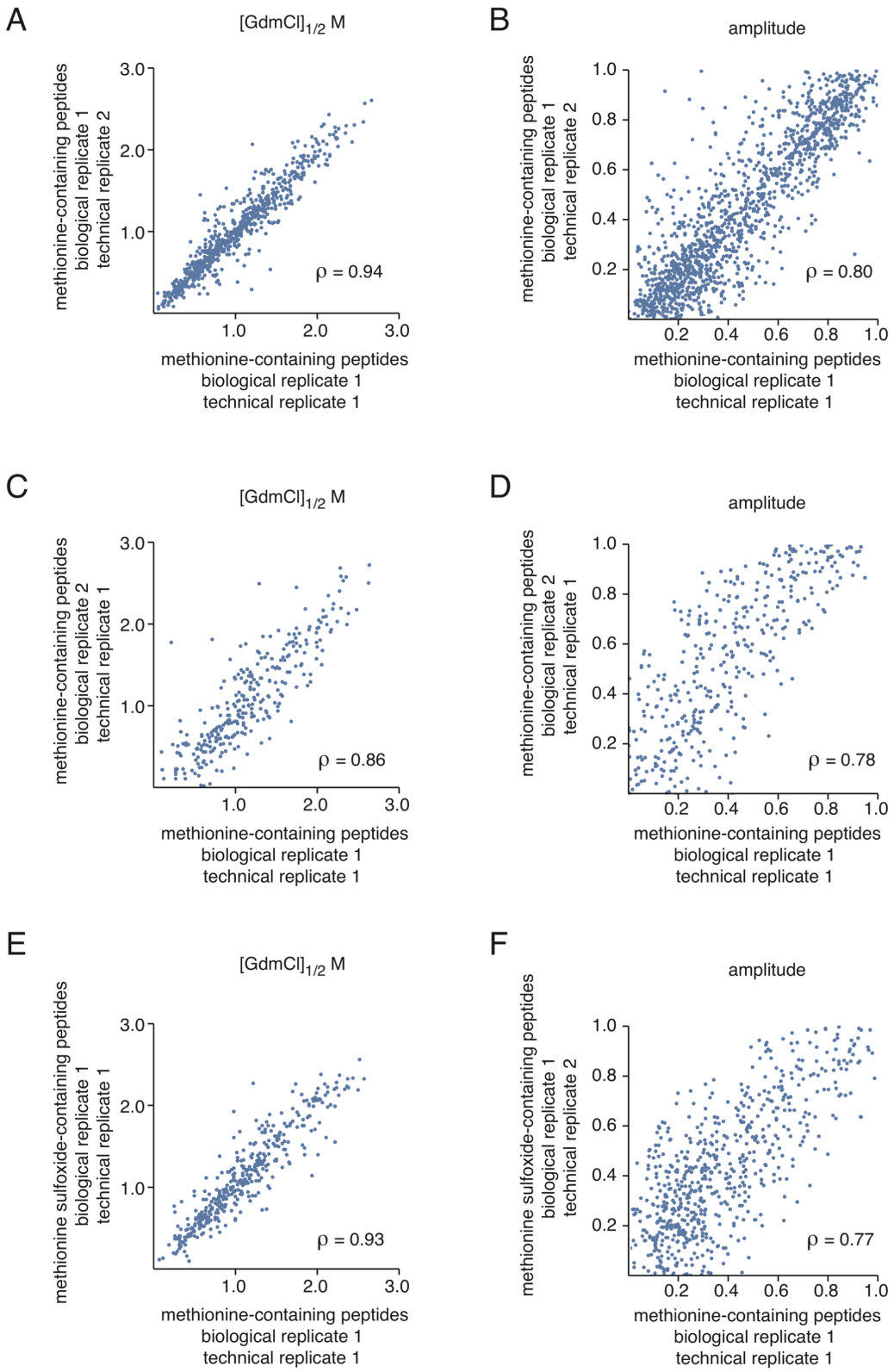
A
[GdmCl]1/2 M
methionine-containing peptides
biological replicate 1
technical replicate 2
methionine-containing peptides
biological replicate 1
technical replicate 1
ρ = 0.94
B
amplitude
methionine-containing peptides
biological replicate 1
technical replicate 2
methionine-containing peptides
biological replicate 1
technical replicate 1
ρ = 0.80
C
[GdmCl]1/2 M
methionine-containing peptides
biological replicate 2
technical replicate 1
methionine-containing peptides
biological replicate 1
technical replicate 1
ρ = 0.86
D
amplitude
methionine-containing peptides
biological replicate 2
technical replicate 1
methionine-containing peptides
biological replicate 1
technical replicate 1
ρ = 0.78
E
[GdmCl]1/2 M
methionine sulfoxide-containing peptides
biological replicate 1
technical replicate 1
methionine-containing peptides
biological replicate 1
technical replicate 1
ρ = 0.93
F
amplitude
methionine sulfoxide-containing peptides
biological replicate 1
technical replicate 2
methionine-containing peptides
biological replicate 1
technical replicate 1
ρ = 0.77

Figure S2

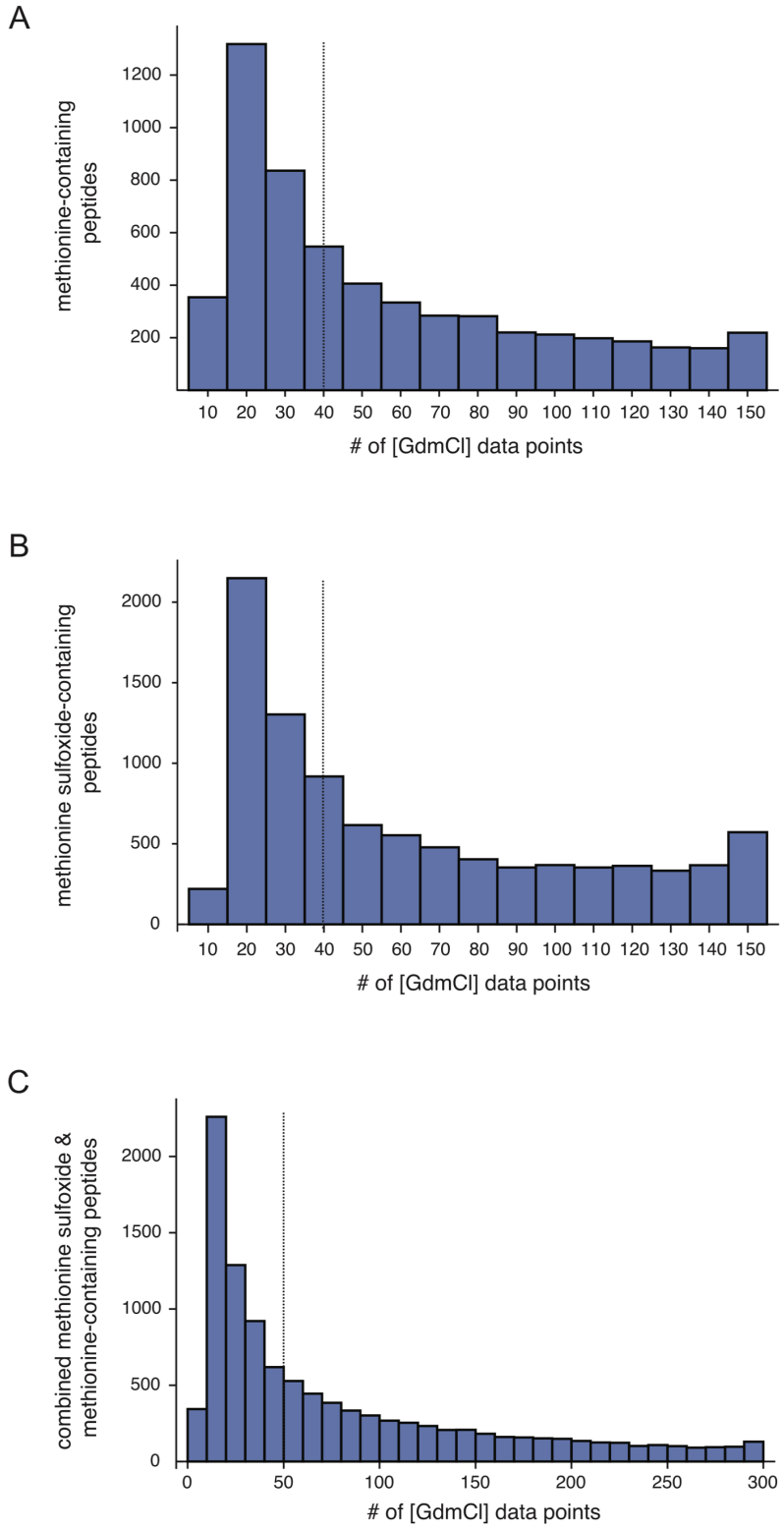
A
methionine-containing peptides
1200
1000
800
600
400
200
10 20 30 40 50 60 70 80 90 100 110 120 130 140 150
of [GdmCl] data points
B
methionine sulfoxide-containing peptides
2000
1500
1000
500
0
10 20 30 40 50 60 70 80 90 100 110 120 130 140 150
of [GdmCl] data points
C
combined methionine sulfoxide & methionine-containing peptides
2000
1500
1000
500
0
0 50 100 150 200 250 300
of [GdmCl] data points

Figure S3

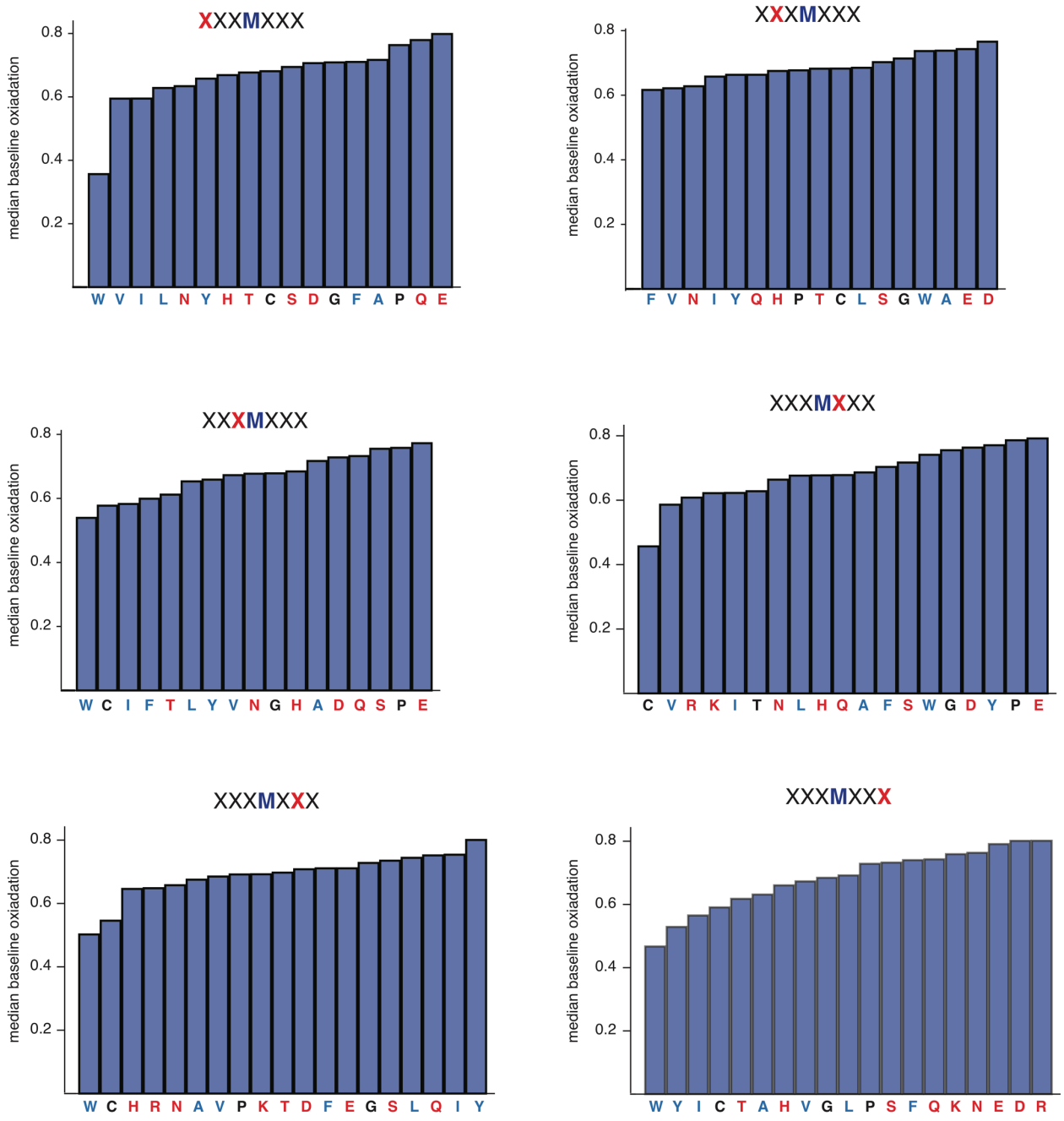
XXXMXXX
median baseline oxiadation
0.8
0.6
0.4
0.2
W V I L N Y H T C S D G F A P Q E
XXXMXXX
median baseline oxiadation
0.8
0.6
0.4
0.2
F V N I Y Q H P T C L S G W A E D
XXXMXXX
median baseline oxiadation
0.8
0.6
0.4
0.2
W C I F T L Y V N G H A D Q S P E
XXXMXXX
median baseline oxiadation
0.8
0.6
0.4
0.2
C V R K I T N L H Q A F S W G D Y P E
XXXMXXX
median baseline oxiadation
0.8
0.6
0.4
0.2
W C H R N A V P K T D F E G S L Q I Y
XXXMXXX
median baseline oxiadation
0.8
0.6
0.4
0.2
W Y I C T A H V G L P S F Q K N E D R

Figure S4

low baseline oxidation

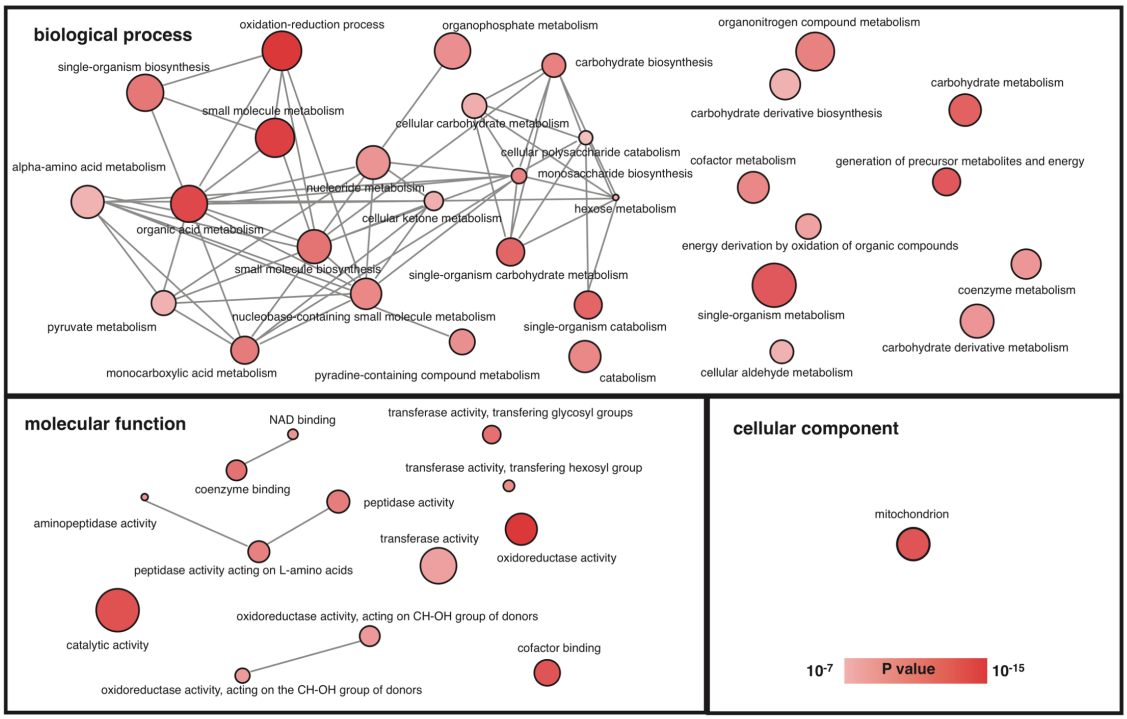

high baseline oxidation

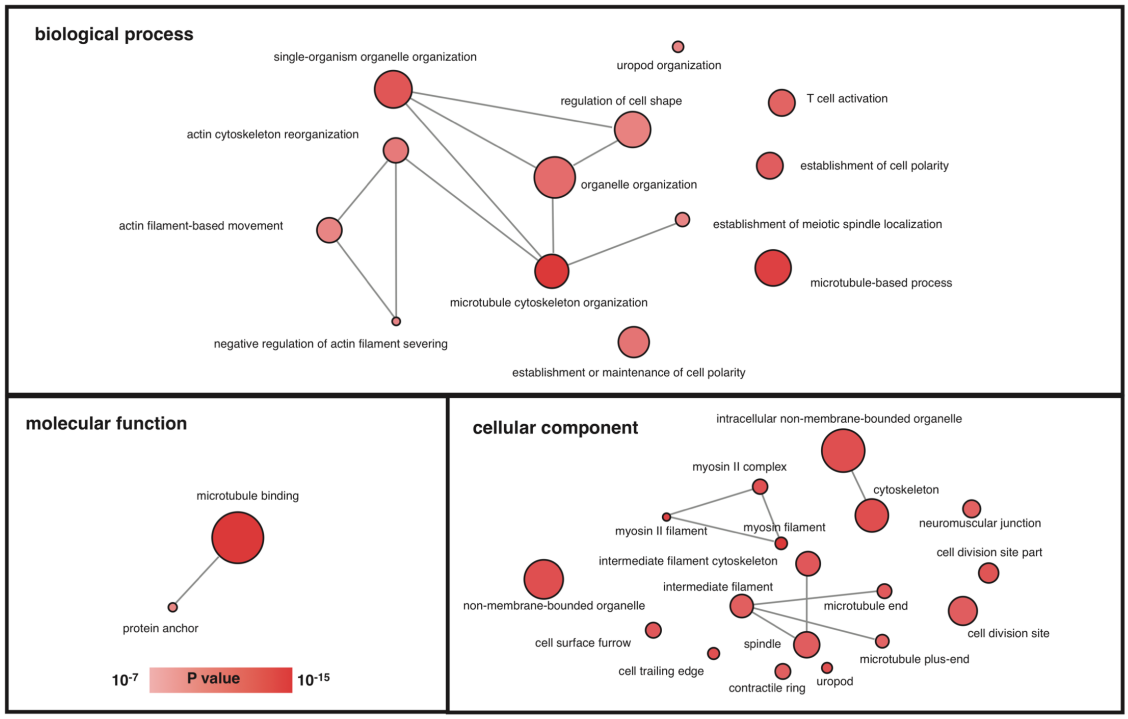

Figure S5

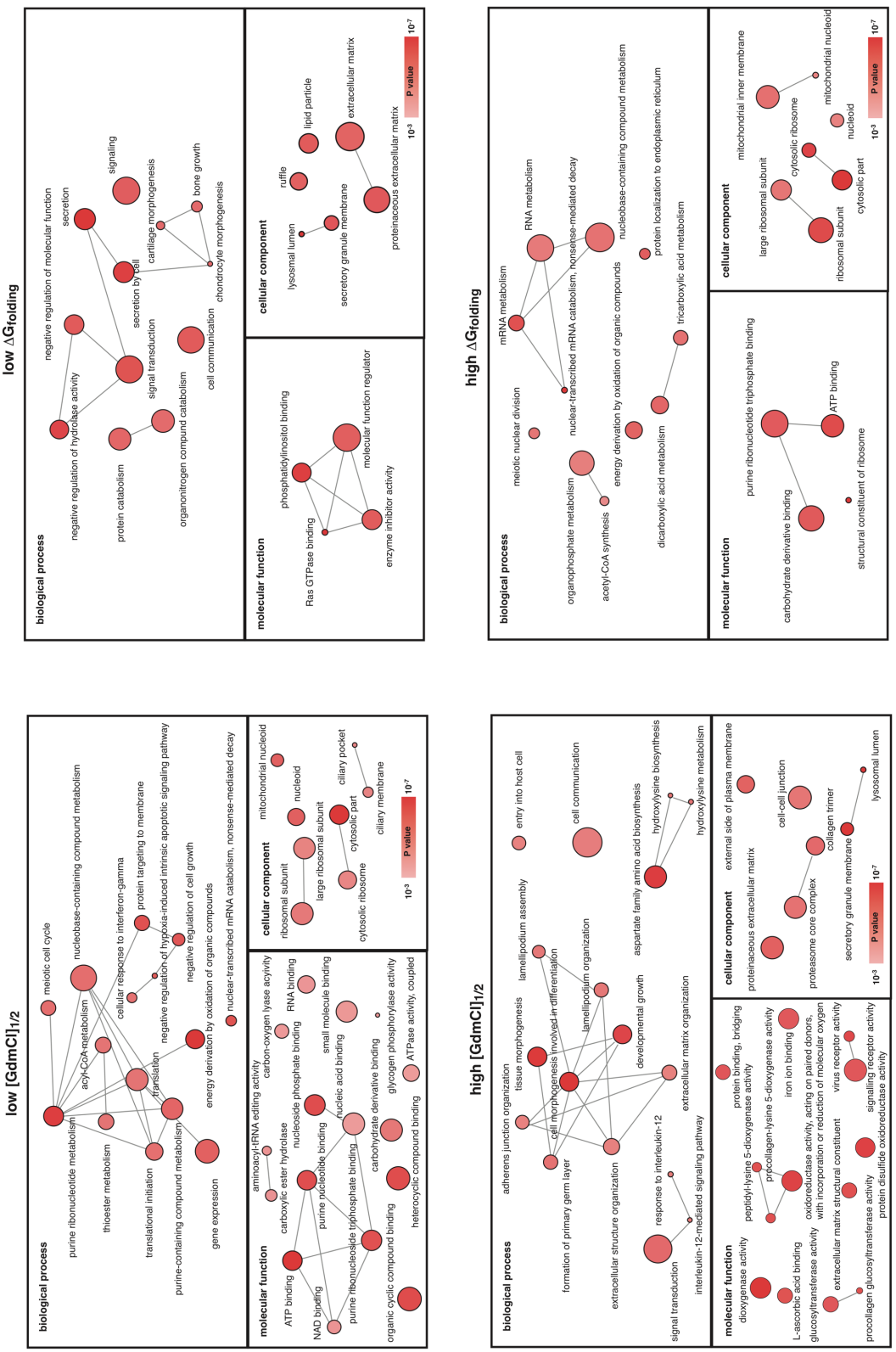
low [GdmCl]1/2
biological process
meiotic cell cycle
nucleobase-containing compound metabolism
purine ribonucleotide metabolism
acyl-CoA metabolism
thioester metabolism
cellular response to interferon-gamma
protein targeting to membrane
translational initiation
translation
negative regulation of hypoxia-induced intrinsic apoptotic signaling pathway
purine-containing compound metabolism
negative regulation of cell growth
energy derivation by oxidation of organic compounds
gene expression
nuclear-transcribed mRNA catabolism, nonsense-mediated decay
molecular function
aminoacyl-tRNA editing activity
carbon-oxygen lyase activity
carboxylic ester hydrolase
RNA binding
ATP binding
nucleoside phosphate binding
NAD binding
purine nucleotide binding
small molecule binding
nucleic acid binding
purine ribonucleoside triphosphate binding
carbohydrate derivative binding
glycogen phosphorylase activity
organic cyclic compound binding
heterocyclic compound binding
ATPase activity, coupled
cellular component
mitochondrial nucleoid
ribosomal subunit
nucleoid
large ribosomal subunit
ciliary pocket
cytosolic part
cytosolic ribosome
ciliary membrane
P value
10-3
10-7
high [GdmCl]1/2
biological process
adherens junction organization
tissue morphogenesis
lamellipodium assembly
entry into host cell
cell morphogenesis involved in differentiation
formation of primary germ layer
cell communication
lamellipodium organization
extracellular structure organization
developmental growth
aspartate family amino acid biosynthesis
hydroxylysine biosynthesis
response to interleukin-12
extracellular matrix organization
hydroxylysine metabolism
signal transduction
interleukin-12-mediated signaling pathway
molecular function
protein binding, bridging
dioxygenase activity
peptidyl-lysine 5-dioxygenase activity
procollagen-lysine 5-dioxygenase activity
iron ion binding
L-ascorbic acid binding
oxidoreductase activity, acting on paired donors, with incorporation or reduction of molecular oxygen
glucosyltransferase activity
extracellular matrix structural constituent
virus receptor activity
signalling receptor activity
procollagen glucosyltransferase activity
protein disulfide oxidoreductase activity
cellular component
external side of plasma membrane
proteinaceous extracellular matrix
cell-cell junction
proteasome core complex
collagen trimer
secretory granule membrane
lysosomal lumen
P value
10-3
10-7
low ΔGfolding
biological process
negative regulation of molecular function
secretion
signaling
negative regulation of hydrolase activity
secretion by cell
cartilage morphogenesis
bone growth
signal transduction
protein catabolism
organonitrogen compound catabolism
cell communication
chondrocyte morphogenesis
molecular function
phosphatidylinositol binding
molecular function regulator
Ras GTPase binding
enzyme inhibitor activity
cellular component
ruffle
lipid particle
lysosomal lumen
extracellular matrix
secretory granule membrane
proteinaceous extracellular matrix
P value
10-3
10-7
high ΔGfolding
biological process
mRNA metabolism
RNA metabolism
meiotic nuclear division
nuclear-transcribed mRNA catabolism, nonsense-mediated decay
nucleobase-containing compound metabolism
organophosphate metabolism
energy derivation by oxidation of organic compounds
protein localization to endoplasmic reticulum
acetyl-CoA synthesis
dicarboxylic acid metabolism
tricarboxylic acid metabolism
molecular function
purine ribonucleotide triphosphate binding
ATP binding
carbohydrate derivative binding
structural constituent of ribosome
cellular component
mitochondrial inner membrane
large ribosomal subunit
cytosolic ribosome
mitochondrial nucleoid
ribosomal subunit
nucleoid
cytosolic part
P value
10-3
10-7

Figure S6

A

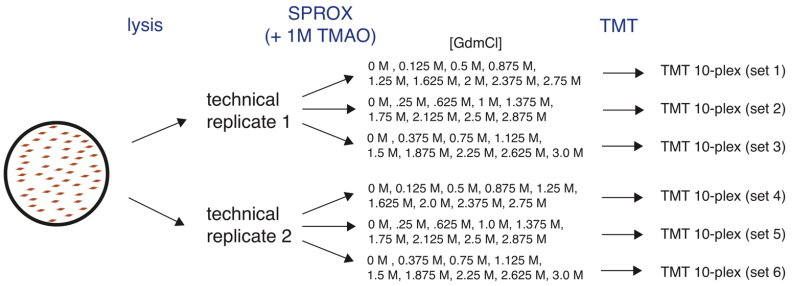

B

Combined proteome coverage of HR-SPROX analyses + 1 M TMAO

incorporated residue	unique peptides	unique proteins
met(unmodified)	5,719	1,977
met(ox)	4,263	1,533
met(unmodified) & met(ox)	2,775	1,169
met(unmodified) or met(ox)	6,077	1,991

C

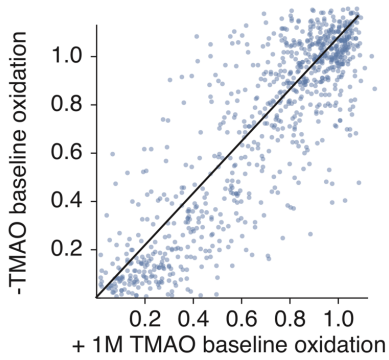

D

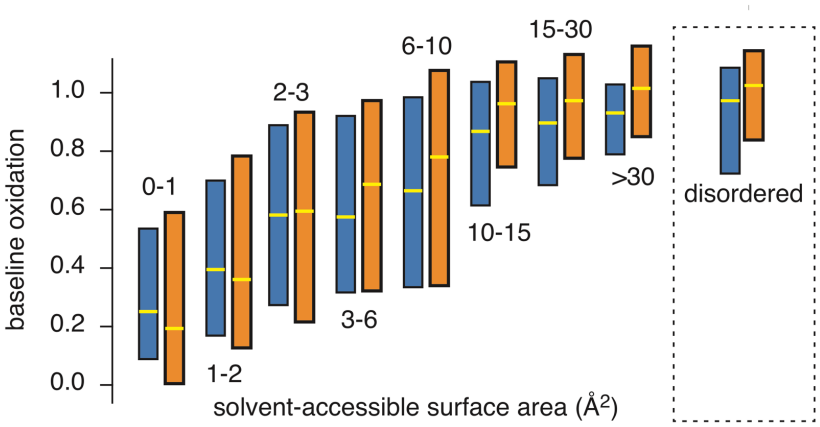

Figure S7

Supplementary Figure Legends

Figure S1. Proteome-wide prevalence of oxidized residues in HR-SPROX data. (A) Relative change in levels of all peptides containing unoxidized versions of each amino acid in the presence and absence of H_2O_2 and GdmCl. The y-axes indicate the median level of all peptides harboring one or more of the indicated residues relative to the level present in unoxidized samples. The data suggest that the oxidation of methionine (leading to decreases in levels of unoxidized methionines) is the most prevalent among all residues and increases as a function of [GdmCl]. The only other unoxidized residue that decreases significantly upon addition of H_2O_2 is cysteine. (B) To identify the oxidized forms of methionines and cystines present in our samples, we searched the proteomic data (technical replicate 1) for methionine sulfoxides (Met-O), methionine sulfones (Met-O_2), sulfenic acid (Cys-O), sulfinic acid (Cys-O_2), and sulfonic acid (Cys-O_3). The bar plot indicates the fraction of methionine- and cysteine-containing peptide sequences in the dataset for which the indicated oxidized forms were also identified. (C) The fraction of the total intensities of the MS1 peaks of methionine and cysteine containing peptides that were mapped to oxidized forms of each peptide. The data shown in B-C indicate that Met-O and Cys-O_3 are the only oxidized forms of methionine and cysteine that are present at significant levels. (D) The change in the relative levels of Met-O and Cys-O_3 as a function of H_2O_2 and [GdmCl] as determined by the fraction of the total intensities of the corresponding MS2 reporter ion peaks mapped to oxidized forms of each peptide. The data indicate that unlike Met-O, Cys-O_3 remains at low constant levels upon increasing GdmCl concentrations. This is likely due to the fact that most oxidizable cysteines are on protein surfaces and their exposure to oxidation is not

influenced by denaturant-induced unfolding. (E) The disappearance of unoxidized met as a function of H_2O_2 and [GdmCl] for met-containing peptides that do or do not contain cystines. The data show that co-occurrence of cystines generally do not alter denaturation curves as monitored by met oxidation. Together, the data in this figure show that met-O is the dominant oxidized species formed in HR-SPROX experiments and although Cys-O_3 is also formed at low levels, it does not artifactually influence the observed oxidation trends for methionine. Relevant to Figure 3.

Figure S2. Pairwise comparisons of replicate HR-SPROX experiments and methionine versus methionine oxide-containing peptides. Data from each replicate experiment were fit to a model-independent sigmoidal equation (equation 1 in Supplementary Information) and amplitudes and $[GdmCl]_{1/2}$ values were measured. The data were compared for pairs of technical (A-B) and biological (C-D) replicates, as well as for methionine and methionine sulfoxide-containing peptides (of the same sequence) within the same experiment (E-F). For each comparison, the Pearson coefficient (ρ) was measured. For all compared data (including comparisons of replicates not shown in this figure), the Pearson coefficient was greater than 0.7. Relevant to Figure 3.

Figure S3. Distribution of the number of denaturation data-points used for HR-SPROX analysis of individual peptides. By combining 15 replicate experiments, we were able to obtain and analyze a large number of data-points (corresponding to different [GdmCl]) for each peptide in our dataset. The histograms indicate the distribution of the number of data-points used for the analysis of methionine-containing peptides (A), methionine sulfoxide-containing peptides (B) and merged data containing

both methionine and methionine sulfoxide-containing peptides (C). The dotted lines indicate the median. Relevant to Figure 3.

Figure S4. Median baseline methionine oxidation levels for peptides with varying methionine-neighboring residues. The bar plots indicate the median baseline oxidation levels for all methionine-containing peptides with specific residues at the specified position (red X) relative to the methionine in the primary sequence. Relevant to Figure 4.

Figure S5. Gene ontologies (GO) enriched in proteins with high or low methionine baseline oxidation levels. GO terms enriched in proteins with high or low methionine baseline oxidation levels were identified and the p-value of the enrichment was calculated as described in Methods (Supplementary Table 6). The most significantly enriched GO terms were visualized by the software ReviGO[63] to remove highly redundant terms and visualize the connectivity of the terms (gray lines). The size of the circles correlates with the number of proteins mapped to the GO term and the color indicates the p-value as shown in the bar scale. Relevant to Figure 4.

Figure S6. Gene ontologies (GO) enriched in proteins with high or low stabilities. GO terms enriched in proteins with high or low $[GdmCl]_{1/2}$ or $\Delta G_{folding}$. Refer to Figure S5 figure descriptions. Relevant to Figure 5.

Figure S7. HR-SPROX analysis of the human fibroblast proteome in the presence of 1M TMAO (A) Schematic representation of the experimental design for HR-SPROX analysis of the human fibroblast proteome in the presence of 1M TMAO, indicating the replicates and denaturant concentrations used in the study. Each technical replicate

consists of 3 complementary sets of GdmCl concentrations tagged with TMT 10-plex reagents. (B) Coverage of proteomic analyses in the presence of 1M TMAO. (C) Pairwise comparison of peptide baseline methionine oxidation levels with and without 1M TMAO. Note that the oxidation levels of highly exposed methionines (top-right of the plot) are not impacted by TMAO. (D) Methionine baseline oxidation levels of highly exposed methionines, and those contained in regions classified as disordered in the MobiDB database, are not highly impacted by TMAO. Relevant to Figure 7.

Supplementary Tables

Supplementary Table 1. MaxQuant Search Parameters

Supplementary Table 2. Experiments and reporter ion definitions (+/- TMAO)

Supplementary Table 3. Peptide search results and reporter ion intensities for all experiments (+/- TMAO)

Supplementary Table 4. Measured folding parameters (+/- TMAO)

Supplementary Table 5. Term mappings for bioinformatic analyses (DSSP, SASA, disorder and Pfam)

Supplementary Table 6. Gene ontology (GO) enrichment data